Stewart, J. A., Anagnostou, E., & Foster, G. L. (2016). An improved boron isotope pH proxy calibration for the deep-sea coral *Desmophyllum dianthus* through sub-sampling of fibrous aragonite. *Chemical Geology*, *447*, 148-160. https://doi.org/10.1016/j.chemgeo.2016.10.029

An improved boron isotope pH proxy calibration for the deep-sea coral *Desmophyllum dianthus* through sub-sampling of fibrous aragonite

Joseph A. Stewart [a,b,*], Eleni Anagnostou [a], Gavin L. Foster [a]

[a] Ocean and Earth Science, National Oceanography Centre, University of Southampton. SO14 3ZH, UK.
[a] National Institute of Standards and Technology, Hollings Marine Laboratory, 331 Fort Johnson Rd, Charleston, SC, 29412, USA
*Corresponding author. Tel: +1 843 725 4833, Email: Joseph.Stewart@noaa.gov

Highlights

- $\delta^{11}B$ of deep sea coral is potentially a powerful tool to reconstruct intermediate depth seawater pH
- Microstructural heterogeneities result in uncertainty in pH derived from bulk skeletal $\delta^{11}B$
- We present $\delta^{11}B$ and trace element composition of micro-sampled fibrous aragonite from *D. dianthus*
- $\delta^{11}B$ of fibres lowest in Mg for each coral reveal a stronger, and better-defined dependence on ambient seawater pH
- *D. dianthus* is an archive of precise palaeo-pH (<0.1 pH units), providing that suitable sampling strategies are applied

Abstract

The isotopic composition of boron ($\delta^{11}B$) in marine carbonates is well established as a proxy for past ocean pH, however, its robust application to palaeo-environments relies on the generation of species-specific calibrations. Existing calibrations utilising the deep-sea coral (DSC) *Desmophyllum dianthus* highlight the potential application of this pervasive species to pH reconstructions of intermediate depth waters. Nevertheless, considerable uncertainty remains regarding the estimation of seawater pH from these bulk skeletal $\delta^{11}B$ measurements, likely resulting from microstructural heterogeneities in $\delta^{11}B$ of *D. dianthus*. To circumvent this problem, thus improving the reliability of the *D. dianthus* $\delta^{11}B$-pH calibration, we present a new $\delta^{11}B$ calibration of micro-sampled fibrous aragonite from this species.

Modern coral specimens recovered from the Atlantic, Pacific, and Southern Oceans, micro-sampled using microdrilling, micromilling, and laser cutting extraction, were analysed for trace element (B/Ca, Mg/Ca, Sr/Ca, and U/Ca) and boron isotopic composition. We find the best calibration against the $\delta^{11}B$ of borate in local ambient seawater (a function of pH and taken from hydrographic data sets; pH range 7.57 to 8.05) utilises $\delta^{11}B$ measurements of fibres with likely slow growth rates and minimal contamination from adjacent microstructures (identified by low Mg/Ca) for each coral specimen. This new calibration exhibits a stronger, and better-defined dependence on ambient seawater pH compared to bulk coral $\delta^{11}B$; $\delta^{11}B_{\mathit{fibre}}$ = (**0.93** ±0.17) × $\delta^{11}B_{borate}$ + (**12.02** ±2.63). We suggest that the majority of the variability in measured $\delta^{11}B$ between replicate bands of fibrous aragonite from a *D. dianthus* specimen can be explained by small incorporation of non-fibrous aragonite and surface impurities during microsampling and growth rate effects. This study confirms the utility of *D. dianthus* as an archive of precise palaeo-pH (±0.07 pH units), provided that suitable sampling strategies are applied.

Keywords: *Desmophyllum dianthus*; deep-sea coral; pH; boron isotopes; trace element; fibrous aragonite

1 Introduction

Intervals of increasing atmospheric CO_2 concentration in the recent and geological past are generally associated with decreases in surface ocean pH following CO_2 incursion into surface waters (Doney et al., 2009; Hönisch et al., 2012). Consequently, there is a pressing need to understand the pathways by which the deep ocean has previously sequestered or released atmospheric carbon (Barker et al., 2010; Burke and Robinson, 2012; Martínez-Botí et al., 2015; Skinner et al., 2010; Thiagarajan et al., 2014) and also the physiological and ecological response of marine calcifying organisms to lower pH; particularly under the other added pressures associated with anthropogenic CO_2 emissions (*e.g.* warming and pollution; Orr et al., 2005; Hoegh-Guldberg et al., 2007). To this end, much attention has been focused on ocean carbonate system proxy development to allow reconstruction of seawater pH in the past. Of particular promise is the boron isotope pH-proxy based on the measurement of the boron isotopic composition (expressed as $\delta^{11}B$, representing the $^{11}B/^{10}B$ ratio of samples relative to the $^{11}B/^{10}B$ of standard NIST SRM 951 in parts per thousand) of marine calcifying organisms (Hemming and Hönisch, 2007). Despite this obvious utility, reliable use of this proxy is predicated on robust calibration of $\delta^{11}B$ measurements of modern marine calcifying organisms to the pH of ambient seawater to account for commonly observed vital effects.

Previous studies have described the systematics of the $\delta^{11}B$ pH-proxy (Hemming and Hanson, 1992; Klochko et al., 2006; Zeebe and Wolf-Gladrow, 2001). Briefly, boron in seawater exists almost exclusively in two phases, boric acid ($B(OH)_3$) and the borate ion ($B(OH)_4^-$), with an isotopic equilibrium fractionation between the two species such that $B(OH)_3$ is enriched by 27.2‰ in the heavier ^{11}B isotope (fractionation factor α_B = 1.0272; Klochko et al., 2006). The relative abundance of these two boron species is pH dependent (Dickson, 1990) and because the isotopic composition of the total boron in seawater ($\delta^{11}B_{sw}$ = 39.61‰; Foster et al., 2010) must be maintained the $\delta^{11}B$ of each species of boron is also a function of pH. $\delta^{11}B$ measurements of marine carbonates show a strong similarity to the boron isotopic

composition of the borate ion ($\delta^{11}B_{borate}$) forming the basis for a model whereby it is the charged borate ion that is predominantly incorporated into $CaCO_3$ (Hemming and Hanson, 1992). This understanding has recently been validated in aragonite using inorganic precipitation experiments (Noireaux et al., 2015).

Boron isotope pH-proxy calibration work to date has predominantly focused on organisms calcifying in the surface ocean including planktonic foraminifera (Henehan et al., 2013; Sanyal et al., 1996; Sanyal et al., 2000) and shallow-water corals (Hönisch et al., 2004; Krief et al., 2010; Reynaud et al., 2004). Yet only limited attention has been given to δ^{11}B-pH calibrations for deep/intermediate dwelling organisms such as benthic foraminifera (Rae et al., 2011) calcitic octocorals (Farmer et al., 2015), and aragonitic deep-sea corals (DSCs; Anagnostou et al., 2012; McCulloch et al., 2012b). Aragonitic DSCs are rich in boron (up to 10 times that of calcitic foraminifera; Blamart et al., 2007; Rae et al., 2011) and of sufficient mass to permit radiometric dating (Cheng et al., 2000; Douville et al., 2010; Lomitschka and Mangini, 1999), making them an attractive substrate for recent intermediate water pH reconstructions.

Corals do not utilise ions derived directly from ambient seawater to build skeletal aragonite; instead corals calcify from a restricted extracellular calcifying fluid (ECF) in the sub-calicoblastic space (Cohen and McConnaughey, 2003), which, although influenced by the external seawater environment, it is primarily controlled by the organism (Comeau et al., 2013; Gagnon et al., 2012; Tambutté et al., 2011). One of the pathways by which the pH and chemical composition of this internal seawater pool is biologically modified is through enzymatic activity (Ca-ATPase pump) transporting Ca^{2+} into the ECF in exchange for H^{+} ions so as to optimise conditions for aragonite precipitation (Al-Horani et al., 2003b; Allemand et al., 2004; Allison et al., 2010; Cohen and McConnaughey, 2003; McConnaughey, 1989; McCulloch et al., 2012b). Thus, the pH of the ECF is often greater than that of ambient seawater (Al-Horani et al., 2003b; Venn et al., 2013), prohibiting estimation of ambient seawater pH derived from coral δ^{11}B measurements by simply applying the theoretical relationship between $\delta^{11}B_{borate}$ and pH (Hemming and Hanson, 1992). Rather, robust,

species-specific, coral $\delta^{11}B$ calibrations to well constrained seawater pH must be implemented for reliable use of this proxy in coral (*e.g.* D'Olivo et al., 2015).

The solitary, azooxanthellate, DSC, *Desmophyllum dianthus* is ideally suited for $\delta^{11}B$-pH reconstructions being both prevalent in the deep ocean and geographically and bathymetrically extensive (up to 70° of latitude and up to 2.5 km water depth; Figure 1; Stanley and Cairns, 1988; Cairns, 1994; Försterra et al., 2005; Thresher et al., 2011). Despite the palaeoceanographic potential of this taxon, recent geochemical studies suggest that DSCs contain considerable microstructural heterogeneity. Optically opaque centres of calcification (COC; Figure 2) generally yield low $\delta^{11}B$ (*e.g.* COC in *Lophelia pertusa* and *Madrepora oculata* respectively up to 8‰ and 3‰ lower; Blamart et al., 2007) and U/Ca ratios, and high Mg/Ca ratios with respect to the adjacent fibrous aragonite that radiates from these internal early mineralisation zones (Gagnon et al., 2007). It is postulated that variable mixing between these different microstructural components is the cause of the relatively large spread in the $\delta^{11}B$ data used in previous attempts to characterise the $\delta^{11}B$-pH relationship for bulk *D. dianthus* (Anagnostou et al., 2012; McCulloch et al., 2012b), limiting the utility of the bulk *D. dianthus* $\delta^{11}B$ proxy to characterising palaeoceanographic-pH shifts (for example the ~0.15 pH unit shift in seawater from last glacial maximum to Holocene; Hönisch et al., 2008; Yu et al., 2010; Rae et al., 2011). It has been suggested that restricting $\delta^{11}B$ analysis to a single microstructural component in DSC specimens, such as the fibrous aragonite, will help to minimise the scatter inherent within the bulk *D. dianthus* $\delta^{11}B$ analyses (Anagnostou et al., 2012), thus allowing the $\delta^{11}B$-pH calibration to be refined and enhance the palaeoceanographic utility of this species. The relatively slow growth-rates of DSCs (*D. dianthus* extension rate up to ~2 mm yr^{-1}; Adkins et al., 2004) and sub-millimetre thickness of fibrous aragonite bands mean that attainment and processing of microstructurally uniform, sub-milligram, DSC samples presents clear challenges. Sampling must be fastidious enough to reject extraneous coralline phases from the fibrous aragonite whilst at the same time ensuring that sample sizes are sufficient for accurate $\delta^{11}B$ analysis (ideally >0.1 mg $CaCO_3$).

Here we present $\delta^{11}B$ data from subsampled fibrous aragonite from the DSC *D. dianthus*. A combination of extraction methodologies are presented and critiqued as to their reliability in obtaining small (sub-milligram) fibre-only samples from DSC, whilst rejecting extraneous skeletal phases. We use these new $\delta^{11}B$ data to explore the potential causes of microstructural heterogeneity in DSCs and to refine bulk *D. dianthus* $\delta^{11}B$-pH calibrations, thereby enhancing the precision and accuracy of intermediate water pH reconstructions.

2 Methodology

2.1 Sampling strategy

Coral samples for this study were obtained from the National Museum of Natural History (Smithsonian Institution, Washington, D.C.) and from the National Institute for Water and Atmosphere (NIWA), Greta Point, Wellington, NZ. The sample set covers a wide variety of depth habitat and latitudinal distribution (Figure 1; Table 1). Only samples collected alive were selected for analyses (*i.e.* with associated organic tissue; excluding specimen 94069) to ensure hydrographic data are as representative as possible. Many of the *D. dianthus* specimens used in this study were analysed for bulk septa $\delta^{11}B$ by Anagnostou et al., (2012) allowing results to be directly compared.

Where necessary calyx subsamples comprising one to two primary S1 septa (Figure 2 A; see Cairns, 1994 for structural nomenclature of solitary scleractinia) were detached using a <1 mm cut-width (diamond coated) rotary blade. The majority of surficial organic matter was mechanically removed from coral septa using a water-pick and a soft brush. Samples were then mounted in an epoxy resin and sectioned parallel to the primary growth axis, orthogonal to the plane of the S1 septa, using a low-speed saw (Buehler®) fitted with a 0.4 mm diamond wafering blade (Figure 2 A). Cut sample surfaces were polished using wetted silicon carbide fixed abrasive papers (Buehler®) to remove surface irregularities. A variety of microsampling approaches were applied here with the shared aim of exclusively sampling coral fibrous aragonite but with sufficient $CaCO_3$ recovery to yield precise $\delta^{11}B$ results. We

now discuss these microdrilling, micromilling and laser cutting approaches in order of decreasing simplicity and speed of sampling (Figure 2 B, C and D).

2.1.1 Microdrilling (large fibre bands)

The surfaces of sectioned corals were wiped with methanol and thoroughly rinsed with MilliQ ultrapure water (18.2 MΩ) to remove dust and surface contaminants. Lines of fibrous aragonite (0.5 to 7 mm length along primary growth axis; 250 µm depth) were then directly microdrilled from cleaned, polished blocks of corals using the ESI New Wave MicroMill and a Brasseler H1621.31.008 Scriber drill bit (cut width 100 µm), leaving approximately 50 µm between the sample area and adjacent COCs or external coating. The resulting powered fibre sample was recovered in a droplet of MilliQ water using an acid cleaned pipette tip. Between samples, residual carbonate dust was removed using compressed air and the drill bit was cleaned in weak acid and rinsed thoroughly in MilliQ water to minimise sample cross-contamination.

Direct microdrilling of fibrous aragonite is desirable because, if performed successfully, this technique avoids powdering the unwanted COCs and external septum coating altogether. In practice however, the narrow diameter drill bit used is susceptible to slipping towards lines of weakness (such as the surface between coral and epoxy), potentially leading to unintentional entrainment of non-fibrous carbonate. Although this occasionally occurred, any samples where non-target COC/coatings were visibly incorporated were rejected. This led to microdrilling being reserved for samples with atypically thick zones of fibrous aragonite (*i.e.* >500 µm thickness).

2.1.2 Micromilling (intermediate fibre bands)

Polished and cleaned sample blocks possessing thinner zones of fibre (100 to 400 µm thick) required a more stable micromilling approach using a broader Brasseler 850 016 drill bit (cut width 800 µm) to provide drill bit stability. For this milling approach, a preliminary sampling trench was drilled into the epoxy at a depth of 300 µm overlapping the outermost 50 µm of the coral to completely remove the external

coating and avoid epoxy contamination of the final milled powder. The sample block was then removed from the stage, thoroughly cleaned again with methanol and MilliQ to remove any drilling residue from the trench, before returning to the stage for sampling. The cleaned drill bit was then used to sample progressively towards the COCs (as finely as 20 µm slices) at a depth in the z-direction of 250 µm. This technique yielded far greater sampling precision for those *D. dianthus* samples with thin fibrous zones.

The progressive nature of sampling by the micromilling technique allowed multiple samples to be extracted across singles band of fibrous aragonite in two *D. dianthus* specimens (19168 and 83583). Radial extension rates in DSCs are complex (Adkins et al., 2004) however, we assume that our sampling approximately 50 µm at a time from the fibres close the sample edge, to the fibres close to COCs represents a general transition from most recent to oldest fibre growth. For these two specimens, once multiple fibre samples had been removed, this progressive sampling was continued to extract a predominantly COC sample for comparison to adjacent fibres.

2.1.3 Laser cutting (small fibre bands)

Laser cutting of fibres was applied to samples with particularly narrow fibre zones (<100 µm thick). The principal advantage of this approach was it allowed even greater accuracy of sampling and enabled the recovery of whole pieces of aragonite (rather than milled/drilled powder) that result in minimal losses during subsequent chemical cleaning. Polished, surface-cleaned, coral thin sections, of uniform 200 µm thickness, were mounted in the New Wave UP193FX Laser Ablation device and individual pieces of fibrous aragonite were detached from the surrounding exterior coating and COC through laser drilling using a 50 µm spot size, 20 Hz, a fluence of ~6 J/cm^2 and scanning speed of 5 µm/sec speed. This laser cutting technique is only recommended for very small samples, owing to its time consuming nature (24 hours to cut one sample) and associated expense.

2.2 Analytical techniques

All analytical techniques used in this study were carried out at the University of Southampton and follow the protocols previously described in Foster (2008). Extracted fibrous aragonite samples, weighing between 60 and 660 µg (typically 300 µg, ~12 ng of B; Table 2), were subject to oxidative cleaning in warm 1% H_2O_2 (buffered in ammonium hydroxide) to chemically remove remaining organic matter. The fibre samples were then given a weak acid leach (0.0005 M HNO_3) to remove any re-adsorbed ions. Once cleaned, samples were dissolved in a minimal volume of 0.5 M HNO_3 before centrifuging and transferring into clean PFA vials.

2.2.1 Elemental analysis

Prior to isotopic analysis, a small aliquot of each sample solution (~7%) was taken for elemental analysis using the Thermo Scientific Element 2 ICP-MS. Aliquots were diluted to an equal concentration of Ca and bracketed by well-characterised, matrix-matched synthetic standard solutions to yield B/Ca, Mg/Ca, Sr/Ca and U/Ca ratios for samples and to assess external reproducibility (2σ uncertainties of B/Ca = ± 5%, Mg/Ca = ± 2%, Sr/Ca = ± 2%, U/Ca = ± 4%). The JCp-1 reference material is a finely powdered coral (<250 µm; crushed by ball mill over 4 days; Okai et al., 2002) that is a similar size fraction to micromilled/drilled samples in this study. Eight identical JCp-1 powders (~5 mg in weight) and nine coarsely powdered samples from bulk *D. dianthus* specimen 19168 (superficially crushed by pestle and mortar; fragments up to ~500 µm) were analysed for trace element chemistry to assess the influence of cleaning; some received oxidative treatment as outlined above and some did not. These trace element values were used to assess the impact of organic matter removal on trace element values and measurement accuracy. Only Sr/Ca ratios measured in JCp-1 were found to be consistently different to those documented in the interlaboratory comparison study by Hathorne et al., (2013), therefore a correction factor of +4.7% is applied to all Sr/Ca results in this study (Table 3). Ancillary Al/Ca, Fe/Ca, and Mn/Ca measurements (2σ respectively ± 8%, ± 7%, and ± 7%) were also made to ensure samples were free from contamination derived from detrital clay (*i.e.*

Al/Ca < 200 µmol/mol) and oxide rich coatings (*i.e.* Fe/Ca < 100 µmol/mol and Mn/Ca < 50 µmol/mol).

2.2.2 Boron isotope analysis

The boron in the remaining sample solutions was separated from the carbonate matrix using 20 µl micro-columns containing Amberlite IRA 743 boron-specific anionic exchange resin (Kiss, 1988). All boron must be recovered from columns to avoid isotopic fractionation, therefore following elution of the boron fraction, additional elutions were checked to ensure >99% of sample boron was recovered in the sample. Resultant solutions for boron isotope analyses used for the δ^{11}B-pH calibration ranged from 3 to 33 ng of boron.

The δ^{11}B of purified boron samples were measured in duplicate on a Thermo Scientific Neptune multi-collector (MC)-ICPMS against NIST SRM 951. The uncertainty on the average of the δ^{11}B of the duplicates is dependent on boron intensity (long-term JCp-1 standard reproducibility for the laboratory while data in this study were collected, estimated using from voltage measured on ^{11}B cup; n>40; typically 500 mV for 35 ppb B) and is calculated as,

$$2\sigma = 1.30\times10^{5}\, e^{-212[^{11}\mathrm{B}]} + 0.34e^{-1.54[^{11}\mathrm{B}]} \qquad (1)$$

A total procedural blank was also measured alongside batches of 8 samples throughout this study. A total procedural blank adjustment was applied to the coral fibre samples, however in all cases the impact on δ^{11}B results was small (*i.e.* less than analytical uncertainty).

2.3 Hydrographic data

For the δ^{11}B-pH calibration we included coral samples only from localities which were in close proximity to well-constrained water sample measurements of alkalinity and dissolved inorganic carbon (DIC) in the CDIAC ocean carbon system database; (http://cdiac.ornl.gov). The *D. dianthus* specimens lacking reliable hydrographic data were reserved for the assessment of microstructural δ^{11}B variability. The

hydrographic alkalinity and DIC data for each coral shown in Table 1 were used in conjunction with temperature, salinity, and nutrient data to calculate pH (total scale), carbonate ion concentration, and aragonite saturation state at each coral location in the Seacarb package in R (Gattuso et al., 2015) using the dissociation constants from Lueker et al. (2000) and the boron/salinity relationship of Lee et al. (2010). Calculated seawater pH values were then used to calculate ambient $\delta^{11}B_{borate}$ rearranging equation (2) (Zeebe and Wolf-Gladrow, 2001) to give equation (3), where α_B is the fractionation factor between boric acid to borate (1.0272; Klochko et al., 2006) and pK_B^* is the dissociation constant of the two boron species calculated using the Seacarb package in R with site-specific temperature, salinity, and pressure data.

$$pH = pK_B^* - \log\left(-\frac{\delta^{11}B_{sw} - \delta^{11}B_{borate}}{\delta^{11}B_{sw} - \alpha_B\delta^{11}B_{borate} - 1000(\alpha_B - 1)}\right) \quad (2)$$

$$\delta^{11}B_{borate} = \frac{\delta^{11}B_{sw} + (\delta^{11}B_{sw} - 1000(\alpha_B - 1))10^{pK_B^* - pH}}{1 + \alpha_B 10^{pK_B^* - pH}} \quad (3)$$

We estimate the impact of anthropogenic CO_2 invasion on pH estimates (*i.e.* Sabine et al., 2004), through subtraction of the accumulated anthropogenic contribution to DIC averaged across a 1° box (±50 m of coral depth) in the GLODAP gridded database (http://cdiac.ornl.gov/oceans/glodap), to be small (typically <0.01 pH units) and can therefore be omitted (Note: 1° box for site 47409 is extended to ±100 m to account for discrepancy between coral sample depth and hydrographic bottle depth). The same 1° boxes from the GLODAP gridded database were used to estimate the local pH variability at each coral locality; calculating multiple pH estimates from each paired value of alkalinity and DIC within the defined box. This method yielded uncertainty in ambient pH of < ±0.05 pH units (2σ) that manifest in uncertainty on $\delta^{11}B_{borate}$ of < ±0.24‰ (Table 1).

3 Results

3.1 Cleaning experiments

Trace element results of peroxide treated and untreated coarsely powdered bulk 19168 *D. dianthus* samples and finely powdered *Porites* coral JCp-1 are shown in (Table 3). Trace element results replicate well within treatments (up to only 3% RSD), suggesting that both of these coarse and finely powdered carbonates were successfully homogenised. No significant difference was observed between trace element values of cleaned and uncleaned *D. dianthus* when coarsely powdered (pestle and mortar; low surface area; low cleaning efficacy), whereas B/Ca and Mg/Ca ratios in finely powdered JCp-1 (ball-milled for 4 days) were seen to decrease by approximately 25% (−113 and −990 µmol/mol respectively) upon removal of organics. Oxidative cleaning was found to have minimal impact on Sr/Ca and U/Ca values in either powdered carbonate.

3.2 $\delta^{11}B_{fibre}$ *vs.* $\delta^{11}B_{borate}$

In Figure 3 A we show previous carbonate $\delta^{11}B$ measurements regressed against the $\delta^{11}B_{borate}$ ambient seawater (a function of seawater pH; Equation 3) including bulk *D. dianthus* $\delta^{11}B$ ($\delta^{11}B_{bulk}$; Anagnostou et al., 2012; McCulloch et al., 2012b), surface corals (Hönisch et al., 2004; Krief et al., 2010; Reynaud et al., 2004; Trotter et al., 2011), and calcitic bamboo octocorals (Farmer et al., 2015). The $\delta^{11}B$ of bamboo corals falls close to the 1:1 line between carbonate $\delta^{11}B$ and $\delta^{11}B_{borate}$ suggesting that these biocalcifiers simply incorporated borate ion from seawater with little modification (Farmer et al., 2015). This is in contrast to bulk *D. dianthus* values that are relatively enriched in ^{11}B with respect to the 1:1 line (by approximately +11‰); more than 2‰ heavier than shallow-water coral taxa growing at equivalent pH (Figure 3; Anagnostou et al., 2012; McCulloch et al., 2012b).

Our new $\delta^{11}B_{fibre}$ and trace element data are shown in Table 2 and $\delta^{11}B_{fibre}$ data are compared in detail to the $\delta^{11}B_{bulk}$ data of Anagnostou et al. (2012) in Figure 3 B. Comparative regression analysis for each of these calibrations are summarised in

Table 4. The majority of $\delta^{11}B_{fibre}$ values fall within 1‰ of $\delta^{11}B_{bulk}$ values where identical specimens were sampled and we find no consistent $\delta^{11}B$ offset between these two data sets. Rather, we document average $\delta^{11}B_{fibre}$ values that are both more than 0.5‰ higher in some cases (samples 19168, 47409, 94069) and lower in others (samples 82065, 48740, 47407) than their respective bulk measurement. Like $\delta^{11}B_{bulk}$ ($R^2 = 0.42$) our new *D. dianthus* $\delta^{11}B_{fibre}$ data are well correlated with $\delta^{11}B_{borate}$ if considered as solitary measurements ($R^2 = 0.48$), with the sensitivity to pH (inferred from the slope of the regression; 0.72) nearly identical to that of $\delta^{11}B_{bulk}$. We note however that if the mean of replicate $\delta^{11}B_{fibre}$ data for each coral sample is taken, the correlation with $\delta^{11}B_{borate}$ improves greatly, with $\delta^{11}B_{borate}$ explaining 69% of the variance in the average $\delta^{11}B_{fibre}$ data. Moreover, filtering these $\delta^{11}B_{fibre}$ data so as to only include the $\delta^{11}B_{fibre}$ sample replicate with lowest measured Mg/Ca (denoted by † symbol in Table 2) further strengthens the correlation with $\delta^{11}B_{borate}$ ($R^2 = 0.83$); yielding a greater sensitivity to pH (steeper slope that is closer to 1) and narrower confidence intervals at the 95% level (Figure 3 B).

3.3 Spatial chemical variability in individual fibres

Systematic changes in $\delta^{11}B_{fibre}$ and trace element variability (B/Ca, Mg/Ca, Sr/Ca and U/Ca) during coral growth were further assessed, using the multiple samples taken across single bands of fibrous aragonite, in *D. dianthus* specimen 19168, possessing the thickest bands of fibrous aragonite and specimen 83583 from the lowest pH site (Figure 4). Sample 1 from 19168 shows decreases in $\delta^{11}B$ and Mg/Ca (of 0.9 ‰ and 0.15 mmol/mol respectively) sampling fibres progressively away from the COCs while Sr/Ca and U/Ca both increase (by 0.63 mmol/mol and 0.15 μmol/mol respectively). The other two specimens measured in this manner (19168 Sample 2 and 83583) show more consistent intra-fibre chemistry, however similar trends are also present in these specimens, particularly $\delta^{11}B$ and U/Ca in sample 83583, with more muted change found in 19168 Sample 2 (Figure 4).

The sampling methods described in this study are not of sufficient spatial resolution to allow the acquisition of a “pure” COC sample containing no fibrous aragonite

component. However, the purest COC sample obtained was from the centre of 19168 Sample 1 that possessed the most prominent COC. This COC sample yielded higher B/Ca (+20%; +42 μmol/mol) and Mg/Ca (+80%; +1.10 mmol/mol), similar Sr/Ca (only 10% or 0.77 mmol/mol lower), and lower U/Ca (−30%; −0.84 μmol/mol) relative to adjacent fibrous aragonite; a finding consistent with previous *D. dianthus* microstructural trace-element studies (Anagnostou et al., 2011; Blamart et al., 2007; Gagnon et al., 2012). The less prominent COC sampled from 83583 does not exhibit any clear chemical differentiation between COC and adjacent fibrous aragonite (with the exception of lower U/Ca in the COC), however the narrower COC sampled here will represent a significant mixing with the fibrous aragonite end member. Despite the disparate trace element chemistry between COC and fibres we observe relatively small differences (<0.9‰; *c.f. Lophelia pertusa* data by Blamart et al., 2007) between $\delta^{11}B$ in fibres and COCs using our sampling strategies (Figure 4; Table 2).

3.4 Trace elements in *D. dianthus* fibres

We compare our new *D. dianthus* $\delta^{11}B_{fibre}$ data to measured trace element ratios for each dissolved fibre sample (Figure 5). *D. dianthus* $\delta^{11}B_{fibre}$ data are positively correlated with B/Ca and Mg/Ca and negatively correlated with Sr/Ca (albeit with a relatively weak correlation) and U/Ca. We note that the strength and direction of trace element correlation to $\delta^{11}B_{fibre}$ appears to be dependent on the partition coefficient of each trace element into aragonite ($D_X = (X/Ca)_{Aragonite}/(X/Ca)_{Seawater}$): Elements that more preferentially remain in solution during the calcification process (*i.e.* B and Mg; *D* values <<1) yield positive correlations. Conversely, elements favourably incorporated into the aragonite lattice (*i.e.* U; *D* value > 1) are negatively correlated with $\delta^{11}B_{fibre}$, while elements incorporated close to unity with seawater (*i.e.* Sr; *D* value only slightly above 1) show the poorest degree of correlation.

There is no systematic trace element or isotopic offset between *D. dianthus* fibrous aragonite sampling techniques with the exception of samples collected via the laser cutting technique that yield anomalously high B/Ca values (+300 μmol/mol)

compared to milled/drill samples of similar $\delta^{11}B$ (Figure 5; Table 2; compare samples from 19249).

4 Discussion

4.1 An improved $\delta^{11}B$-pH calibration for *D. dianthus*

In line with previous DSC studies (Anagnostou et al., 2012; McCulloch et al., 2012b), our total dataset yields a skeletal coral $\delta^{11}B$ to $\delta^{11}B_{borate}$ slope of <1 (Table 4). Together, our new *D. dianthus* data support suggestions that the pH of the calcifying fluid in this DSC is biologically upregulated (Anagnostou et al., 2012; Blamart et al., 2007; McCulloch et al., 2012a), promoting calcification and partially mitigating the effects of the low aragonite saturation states (Ω_{Arag}) found in the deep waters these taxa inhabit (Guinotte et al., 2006).

If our new fibre data are considered as solitary measurements, these data appear similar to absolute $\delta^{11}B$ values of bulk septa and exhibit a similar sensitivity to pH (Figure 3; Table 4). The calibration by linear regression of $\delta^{11}B_{fibre}$ to $\delta^{11}B_{borate}$ has a comparable spread in its residuals (R^2 = 0.48) to that of $\delta^{11}B_{bulk}$ (R^2 = 0.42) suggesting that $\delta^{11}B_{fibre}$ data provide seemingly little improvement to the original $\delta^{11}B_{bulk}$-pH calibration. Yet, if replicate $\delta^{11}B_{fibre}$ data for each coral sample are averaged the $\delta^{11}B_{fibre}$ calibration (R^2 = 0.69) reveals a marked improvement upon the $\delta^{11}B_{bulk}$ calibration. Once averaged, each point on the average $\delta^{11}B_{fibre}$ calibration represents a different mass of averaged fibre $CaCO_3$ (between 0.25 and 1.44 mg). An alternative regression, weighted by fibre sample mass, further improves the calibration (R^2 = 0.76) with minimal impact on the slope or intercept of the regression.

The benefits to the $\delta^{11}B$-pH calibration of microsampling fibrous aragonite in *D. dianthus* are clear, yet the approach of averaging $\delta^{11}B_{fibre}$ data described above still encompasses all of the chemical variability within fibre replicates; the source of which we explore in detail in Section 4.2. Low Mg/Ca ratios in *D. dianthus* substructures are indicative of the purest fibrous aragonite (Gagnon et al., 2007)

and/or slow growth rates (*e.g.* inorganic aragonite; Gabitov et al., 2008; and corals; Montagna et al., 2014). Therefore, when we take full advantage of our microsampling approach and filter our $\delta^{11}B_{fibre}$ data to include only those replicates with the lowest Mg/Ca value (denoted by † in Table 2), we improve the calibration further with $\delta^{11}B_{borate}$ explaining 83% of the variance and suggesting a stronger sensitivity to pH than $\delta^{11}B_{bulk}$ measurements (*i.e.* greater slope). It is presumed the lowest Mg/Ca fibre samples are least contaminated by Mg-rich COCs and were formed closest to thermodynamic equilibrium. We note that the majority of these low-Mg fibre replicates also correspond to high U/Ca further suggesting that these samples are largely free from COC contamination.

This low-Mg $\delta^{11}B_{fibre}$ calibration for pH is a considerable improvement upon the $\delta^{11}B_{bulk}$ calibration (residual standard error of 0.44 and 0.93 respectively); therefore this clearly enhances the utility of the *D. dianthus* calibration permitting yet smaller perturbations in intermediate water pH in the past to be resolved (*e.g.* ~0.15 pH unit shift from last glacial maximum to Holocene changes in seawater pH; Hönisch et al., 2008; Yu et al., 2010; Rae et al., 2011). Application of our new low-Mg fibre calibration to typical coral $\delta^{11}B$ measurements of ~26‰, the 95% confidence intervals suggest that seawater pH can be reconstructed to within ±0.07 pH units (*c.f.* $\delta^{11}B_{bulk}$ ±0.34 pH units). Based on these results, for the most accurate $\delta^{11}B$-pH estimates using this taxon, we suggest one of the following approaches are followed: (i) Multiple fibre replicates are taken (n>3) for paired $\delta^{11}B$ and trace element analyses so that samples with slow growth rates and/or minimal COC contamination (low Mg/Ca, high U/Ca) can be selected for pH estimation based on equation 4;

$$\delta^{11}B_{low\text{-}Mg\ fibre} = (\mathbf{0.93} \pm 0.17) \times \delta^{11}B_{borate} + (\mathbf{12.02} \pm 2.63) \quad (4)$$

(ii) Alternatively, if elemental data are unavailable, powders from these multiple fibre replicates should be combined to make an average fibre sample (ideal total sample mass >0.7 mg; average of this study) and pH should be estimated using the (sample mass weighted) average fibre regression (equation 5).

$$\delta^{11}B_{fibre} = (\mathbf{0.75} \pm 0.17) \times \delta^{11}B_{borate} + (\mathbf{14.69} \pm 2.57) \quad (5)$$

Although low-Mg $\delta^{11}B_{fibre}$ data have clear benefits when it comes to reconstructing accurate seawater pH in the following section we seek further explanation for $\delta^{11}B_{fibre}$ variability within single coral calyxes.

4.2 Causes of $\delta^{11}B$ variability within fibrous aragonite

Measurements of $\delta^{11}B_{fibre}$ and trace element composition across single bands of fibrous aragonite in *D. dianthus* specimen 19168 Sample 1 (and to a lesser extent 19168 Sample 2 and 83583) show that fibre chemistry is not homogenous across a single band of fibrous aragonite (Figure 4). Rather, trace element and isotopic data show trends of decreasing $\delta^{11}B$ and Mg/Ca and increasing Sr/Ca and U/Ca towards the exterior of the septum. Possible sources of $\delta^{11}B_{fibre}$ and trace element variation include (i) site specific differences in hydrography and food supply during growth, (ii) contamination of fibrous aragonite samples with organic matter, COC, or coating during sampling, (iii) Rayleigh fractionation, and/or (iv) growth rate induced changes in skeletal chemistry during calcification. Below we discuss the extent to which these possible sources of variability explain our trace element and isotope data from *D. dianthus* fibres.

4.2.1 Changes in hydrography or food supply during growth

Cold-water corals are known to change their distribution and calcification rates depending on temperature and/or nutrient availability (Dodds et al., 2007; Mienis et al., 2014; Mortensen et al., 2001; Roberts et al., 2006), hence it is possible that *D. dianthus* $\delta^{11}B$ is influenced by hydrographic variables other than pH alone. We therefore explore our $\delta^{11}B_{fibre}$ data for further correlation with ambient seawater conditions. To this end, we regress residuals of the ordinary least squares regression of $\delta^{11}B_{fibre}$ *vs.* $\delta^{11}B_{borate}$ against hydrographic variables such as temperature, salinity, and $[PO_4^-]$, yet we find no significant relationships (residuals *vs.* Temperature, $R^2 < 0.01$; Salinity, $R^2 = 0.01$; $[PO_4^-]$, $R^2 = 0.01$; Supplementary Figure S 1). Further, the amount of variance observed for replicate $\delta^{11}B_{fibre}$ results in each *D. dianthus* sample

bears no clear relation to the variance in the available hydrographic data (Supplementary Figure S 2).

The ability of a DSC to upregulate internal pH could be limited by metabolic energy availability (Al-Horani et al., 2003a), hence food supply may in part drive pH upregulation and therefore some of the $\delta^{11}B_{fibre}$ variability. Yet, we find no clear evidence for food supply (either amount or intra-annual variability estimated from site specific particulate organic carbon flux) driving discrepancies between $\delta^{11}B_{fibre}$ replicates (See Supplementary information).

4.2.2 Contamination of fibres with organics, COC, or surface coating

It was important that organic phases were effectively eradicated from biogenic carbonate samples in this study to ensure these trace-element-rich phases were excluded (*i.e.* high Mg; Barker et al., 2003), and to preserve the micro-columns used for boron purification. The importance of effective oxidative cleaning on coral samples is clear when we compare trace element data from the cleaned and uncleaned JCp-1 standard (Table 3). Our warm buffered peroxide treatment greatly reduced resultant B/Ca and Mg/Ca ratios of this finely powdered standard (*e.g.* Holcomb et al., 2015), suggesting that coral organic phases are potentially rich in these two trace elements and that oxidative cleaning must be applied to extract trace element ratios representative of the aragonite phase. We note that trace element ratios of JCp-1 replicates cleaned in this manner are remarkably consistent (*i.e.* within instrumental analytical uncertainty) suggesting that the cleaning method detailed above yields near-complete and reproducible removal of organics matter in samples.

All micromilled and microdrilled samples in this study were finely powdered (similar surface area to the JCp-1 standard) and therefore we assume successfully eradicated of organics. The lower B/Ca ratios measured in cleaned micromilled/drilled *D. dianthus* samples in this study (300 µmol/mol) compared to *in situ* analyses (e.g. laser-ablation where pre-cleaning was not applied; Montagna et al., 2005) in this species are consistent with a boron rich organic phase being removed. The controls

on the boron isotopic composition of coral organic matter are likely complex. Although light ^{10}B is preferentially adsorbed onto organic surfaces (~25‰ lower than the ambient fluid at pH 8; Lemarchand et al., 2005), the study by Stoll et al. (2012) on coccolithophorids points to membrane permeable boric acid (^{11}B enriched with respect to seawater) as the major source of boron in organic cells. Despite large reductions in B/Ca, results of a recent interlaboratory comparison study reveal only a small reduction in $\delta^{11}B$ of JCp-1 powder (−0.2‰) from oxidative cleaning (Gutjahr et al., 2014), also suggesting that, at least in this case, boron in coral organic matter is isotopically heavier than skeletal carbonate. Although well homogenised, the bulk 19168 sample, superficially crushed by pestle and mortar (large fragments), yielded no such reduction in B/Ca or Mg/Ca after cleaning (Table 3), suggesting that the low surface area of this test sample hindered the efficacy of organic matter removal. Persistence of organic matter in coarse samples likely explains higher B/Ca values measured in *D. dianthus* fibres sampled via the laser cutting methodology in this study (Figure 5) that were similarly cleaned as larger intact fragments. Presence of residual organic phases that are both rich in boron and isotopically heavy may explain why in some cases bulk $\delta^{11}B$ values for *D. dianthus* samples (also homogenised by pestle and mortar; Anagnostou et al., 2012) are higher than $\delta^{11}B_{fibre}$ measurements in this study. The laser cut $\delta^{11}B_{fibre}$ value of sample 19249 falls within the range of microdrilled aliquots of the same sample (only 0.3‰ apart), suggesting that, in this case, $\delta^{11}B_{fibre}$ values are impacted little by choice of microdrilling or laser cutting protocols. While these two laser-cut data points cannot account for the $\delta^{11}B$ variability in the majority of samples that were micromilled/drilled and effectively oxidised, this further suggests that samples collected by laser cutting be used with caution.

If *D. dianthus* corals are chemically similar to the DSC *Lophelia pertusa*, then varying proportions of COCs (Blamart et al., 2007) will cause significant shifts in measured $\delta^{11}B_{fibre}$ values. Special care was made to avoid COCs with the fibrous aragonite sampling strategies described above; certainly in comparison to previous bulk sampling approaches (Anagnostou et al., 2012; McCulloch et al., 2012b).

Additionally, our stringent quality control of sampling protocols ensured that any sample where it was visible that COC had been mistakenly incorporated was rejected prior to analysis. Nevertheless, because filtering of $\delta^{11}B_{fibre}$ data based on Mg content has significant impacts on the calibration with pH, it is conceivable that small amounts of COC are unavoidably incorporated into the micro-samples simply due to averaging of unseen skeletal material in the z-direction and the possibility that minor COCs were not visible on the polished surface. In the *D. dianthus* specimen 19168 these opaque COC bands were found to be similar to adjacent fibre samples differing by less than 0.9‰ in $\delta^{11}B$ composition, despite the large trace element shifts mentioned above (Figure 4). Although analytical techniques are different and our spatial sampling resolution is greatly averaged in comparison to ion microprobe analysis, we suggest that at least for this coral specimen, the difference in $\delta^{11}B$ between COCs and fibres in *D. dianthus* is far smaller than that measured in *Lophelia pertusa* (Blamart et al., 2007). In this regard, we suggest that *D. dianthus* is perhaps more akin to the DSC *Madrepora oculata* for which more minor (~3‰) microstructural differences are reported (Rollion-Bard and Blamart, 2014). Despite only modest differences measured between $\delta^{11}B$ of COC and fibrous aragonite in *D. dianthus*, we document considerable improvement in the $\delta^{11}B$-pH calibration by removing the high-Mg analyses presumably contaminated by COC microstructures. This suggests that the current poorly constrained relationship of bulk skeletal $\delta^{11}B$ to seawater pH in *Lophelia pertusa* (McCulloch et al., 2012b) could be equally improved by applying similar sampling techniques to this microstructurally heterogeneous taxon.

Fibrous aragonite samples where the microdrill track was seen to visibly deviate into (or close to) the line of weakness between the sample edge and surrounding epoxy were considered potentially contaminated by oxide-rich sample coatings and therefore not included in the $\delta^{11}B$-pH calibration. However, analysis of coating contaminated samples such as these reveal measured $\delta^{11}B$ to be up to 3‰ lower than "pure" adjacent fibres samples while deviating little in B/Ca and other trace element chemistry (see 47413 and 94069 "Coating"; Table 2). In light of the detrimental

effect of coating contamination on $\delta^{11}B_{fibre}$ measurements, our sampling techniques focused on the exclusion of these coating phases. High Fe/Ca and Mn/Ca (>200 and >50 μmol/mol respectively) measurements in the 94069 "Coating" sample show that these ancillary data are useful diagnostic tools for identifying substructures strongly contaminated by oxide coatings, however this is not the case for all coating contaminated samples (*e.g.* 47413 "Coating"). Therefore, in a similar argument to that of potential COC contamination, while trace contamination of coating phases in our "pure" fibre samples cannot be discounted, diligent sampling protocols make it unlikely that the spread in replicate $\delta^{11}B_{fibre}$ measurements is down to incorporation of contaminants alone.

4.2.3 Rayleigh fractionation during growth

Spatial chemical profiling across bands of fibrous aragonite reveals that the presumed oldest fibre growth close to COCs has high $\delta^{11}B$ and Mg/Ca and low Sr/Ca and U/Ca with respect to presumed newer growth close to the edge of the septum (Figure 4). Such co-varying chemical trends are echoed more generally across the entire fibrous aragonite data set with the concentration of elements more preferentially incorporated into the aragonite lattice with respect to seawater (*i.e.* U) being inversely correlated with $\delta^{11}B$ while elements less readily incorporated into the coral (*i.e.* B and Mg) are positively correlated with $\delta^{11}B$ (Figure 5). The implied dependency of these elemental-isotopic relationships on partition coefficients suggests a common systematic effect on these parameters during calcification; one candidate for this is Rayleigh fractionation.

Restricted flow of ions from ambient seawater to the ECF leads to Rayleigh-type fractionation as progressive precipitation of skeletal aragonite leaves the residual ECF proportionally enriched/depleted in its elemental ratios to calcium depending on the partition coefficient of the trace element in question. For example, the D_B into aragonite from seawater is <<1, therefore the B/Ca ratio of the residual calcification fluid increases as progressively more aragonite is precipitated with a B/Ca ratio lower than the parent fluid. In this example, later forming aragonite precipitating from this

fluid would have a higher B/Ca ratio than the initial precipitate. Previous Mg/Ca and Sr/Ca measurements by isotope dilution ICP-MS in *D. dianthus* fibrous aragonite are shown to track a closed system type Rayleigh fractionation model (Figure 6 A; Gagnon et al., 2007) hence we apply this closed system model to assess the extent to which simple Rayleigh-type processes can explain Mg/Ca, Sr/Ca, B/Ca and $\delta^{11}B$ variability within the fibrous aragonite samples in this study (see Supplementary information for model description).

The exact fraction of Ca remaining in the ECF relative to ambient seawater concentration for each stage of fibrous aragonite calcification is an unknown therefore, following the approach of Gagnon et al. (2007), we cross-plot the replicate Mg/Ca and Sr/Ca data for specimens with many replicates from sites 19168, 45669, 47413, and 47407 (Figure 6) to assess the fit to the Rayleigh models. Unlike the data from *D. dianthus* sample 47407 measured by Gagnon et al. (2007), fibrous aragonite Mg/Ca and Sr/Ca data in this study do not fit well to Mg:Sr Rayleigh fractionation curves and in many cases show the opposite trend (i.e. positive correlation) to that predicted by Rayleigh fractionation. This further suggests that contaminant phases such as Mg-rich COCs are not being fully rejected by our microsampling techniques. Fibrous aragonite Sr/Ca ratios in this study are generally lower (by ~1 mmol/mol) than Sr/Ca measurements in sample 47407 by Gagnon et al. (2007). The offset in Sr/Ca may, in part, represent discrepancies between analytical techniques, however these samples are difficult to compare directly. It remains unclear if our sample from site 47407 was taken from a different coral calyx and therefore calcifying from entirely different ECFs (perhaps with a subtly lower initial [Sr] in the ECF; −5%; Figure 6 A). Where fibrous aragonite was sampled similar to Gagnon et al. (2007), sequentially across the same fibre band of sample 19168 (Figure 4; black squares Figure 6 A), Mg/Ca and Sr/Ca data cluster tightly and do fit a Rayleigh distribution albeit with very much lower initial [Sr] in the ECF (−15%). This result suggests that initial [Sr] in the ECF can be modified from ambient seawater and is variable between individuals.

Rayleigh models using low estimates for D_B similar to inorganic aragonite (0.0037; Mavromatis et al., 2015; Holcomb et al., 2016) and an initial boron concentration in the ECF equal to ambient seawater are unable to describe the measured B/Ca and $\delta^{11}B_{fibre}$ results, incorporating far too little boron into the skeleton at each iterative step to cause and appreciable shift the residual $\delta^{11}B$ of the ECF and $\delta^{11}B_{fibre}$ (example data from sample 19186 plotted in Figure 6 B). We note that the coral boron chemistry measured in this study can only be defined by tuning the Rayleigh model to unrealistically high D_B (~0.23; two orders of magnitude greater than inorganic aragonite) and with an initial boron concentration in the ECF (7 μM) approximately 60 times lower than $[B]_{sw}$ (432.6 μM; Lee et al., 2010). Alternatively, it is possible that a biological process that strongly rejects seawater boron from the ECF would cause large isotopic fractionation of internal $\delta^{11}B_{sw}$, but varying the starting $\delta^{11}B_{sw}$ in the modelled ECF between 35 and 45‰ does little to alter the gradient of the Rayleigh curve; merely shifting the modelled output up/down the *x* axis. Furthermore, addition of active Ca^{2+} pumping into the ECF (up to 10% replacement of precipitated Ca^{2+}) can only go part way towards increasing the rate at which $\delta^{11}B_{fibre}$ values increase with respect to B/Ca (shaded region Figure 6 C), hence major reduction of the initial [B] in the ECF and extremely high D_B values are still required.

Rare earth element spiked seawater culture experiments suggest that seawater transport to coral calcification sites is direct and rapid (Gagnon et al., 2012). Therefore, without a mechanism to account for such strong biological modification of D_B and [B] in the ECF, we must assume that the impact of Rayleigh fractionation on fibre boron chemistry is small.

4.2.4 Growth rate effects

Given that Rayleigh fractionation is an unlikely driver of the patterns we observe, an alternative explanation is suggested whereby elemental and isotopic variability are the result of two distinct but related mechanisms; seawater pH and crystal growth rate. While seawater pH is a clear driver of the $\delta^{11}B$ in fibrous aragonite, pH also strongly covaries with Ω_{Arag} (Table 1). High saturation states in seawater boost

carbonate precipitation rates (Hoegh-Guldberg et al., 2007) which in turn promotes kinetic disequilibrium at the crystal surface, leading to "growth entrapment" of trace elements that would typically be rejected from the lattice (i.e. B and Mg; $D<<1$; Watson, 2004). A strong dependency on growth-rate has been observed for boron incorporation into inorganically precipitated aragonite (Mavromatis et al., 2015; Noireaux et al., 2015). The decrease in Mg/Ca (and to a lesser extent B/Ca) paired with increases in Sr/Ca and U/Ca from the presumed oldest to the newest fibres, are potentially a result of a progressive decrease in calcification rate from the COC towards the sample edge as the septum is thickened. This change is also supported by the potential decrease in U/Ca-reconstructed carbonate ion concentrations (i.e. calibration by Anagnostou et al., 2011). It is likely therefore that the proposed change in growth rate is associated with a decrease in carbonate ion saturation state within the ECF over time (Holcomb et al., 2009), with the rate of change expected to be related to ambient seawater Ω_{Arag}. This mechanism would also explain the more muted elemental offsets between fibres and COC in specimen 83583 as growth rates presumably remained slow throughout its life at this low pH site.

5 Conclusions and implications

Sample size and shape dictates the choice of fibre sampling technique required to extract exclusively fibrous aragonite sub-samples from a *D. dianthus* calyx. Where possible we recommend the (broad drill bit) micromilling technique be used as it offers high sampling precision over (fine drill bit) microdrilling, without the cost and time burden of laser cutting.

Analyses of bulk carbonate *D. dianthus* samples yield a wide spread in measured $\delta^{11}B$ (Anagnostou et al., 2012; McCulloch et al., 2012b) that are likely the result of both microstructural heterogeneities (*i.e.* Blamart et al., 2007) and inherent variability in skeletal aragonite possibly linked to the calcification mechanism. Although microsampling proves a more labour intensive alternative, if regions within the coral with slow growth rate and/or minimal COC contamination are selected (*i.e.* low-Mg fibres), our $\delta^{11}B$ data yield a more refined calibration against seawater pH in

comparison to similar bulk sampling. Our new calibration therefore boosts the utility palaeoceanographic of *D. dianthus* as a substrate for intermediate water pH reconstruction, allowing shifts of < 0.1 pH to be fully resolved (*e.g.* LGM to Holocene).

6 Acknowledgements

We thank Stephen Cairns (Smithsonian Institute) and Liz Sikes (Rutgers University) for providing sample material and Stephanie Henson for providing POC flux data. SeaWiFS data were provided by GSFC/NASA in accordance with the SeaWiFS Research Data Use Terms and Conditions Agreement. We also thank Clive Trueman, Andy Milton and Matt Cooper (University of Southampton) for their help with laboratory work. We thank the anonymous reviewers and the editor who provided constructive feedback that substantially improved an earlier version of the manuscript.

Financial was supported provided by the Natural Environment Research Council [grant number NE/J021075/1].

689

690 Figure 1: Locations of the *D. dianthus* specimens used in this study. Map created using
691 Ocean Data View software (R. Schlitzer, 2015, http://odv.awi.de)

692

693 Figure 2: Sampling of DSC fibrous aragonite. Panel A: Sectioning of DSC septa to expose
694 target fibrous aragonite along with centres of calcification (COC) and edge coatings. Light
695 microscope image of coral sample 19186 used in this study. Panels B, C and D show
696 different sampling techniques of polished sections described in the text. Microdrilling (B):
697 direct drilling of fibres using fine drill bit to collect powdered sample. Micromilling (C):
698 drilling and initial sampling trench (green) before milling towards fibre samples (yellow)
699 using broad drill bit. Laser cutting (D): repeated laser shots are used to cut whole fibre
700 section from a thin section of 200µm thickness.

701

702 Figure 3: Measured $\delta^{11}B$ of coral regressed against the $\delta^{11}B_{borate}$ of ambient seawater. Panel
703 A. $\delta^{11}B$ of bulk *D. dianthus* (Anagnostou et al., 2012), tropical corals (Hönisch et al., 2004;
704 Krief et al., 2010; Reynaud et al., 2004; Trotter et al., 2011), and bamboo coral (Farmer et
705 al., 2015). Grey dashed parallel lines in show 1:1 $\delta^{11}B$ relationship and the same
706 relationship offset by +11‰. Panel B. (inset of A) shows new fibrous aragonite *D. dianthus*
707 data in comparison to bulk *D. dianthus* (Anagnostou et al., 2012). Open blue symbols
708 represent drilled (triangles), milled (circles) and laser cut fibres (crosses) sampling
709 techniques (error bars show 2σ of each replicate). Filled blue symbols highlight the *D.*
710 *dianthus* fibre replicate with the lowest Mg/Ca. Regression lines are least squares
711 regression models and their 95% confidence intervals (shaded envelopes) for bulk and low
712 Mg/Ca fibre data.

713

714 Figure 4: $\delta^{11}B$ and trace metal composition across bands of fibrous aragonite in *D. dianthus*
715 corals 19168 and 83583 (low pH site) sampled by micromilling from presumed newest to
716 oldest fibre growth. The positions of sample trenches are highlighted in green; subsequent
717 samples are then shown in yellow. The positions where COC samples were also taken are
718 delineated by the connected white circles.

719

720 Figure 5: *D. dianthus* $\delta^{11}B_{fibre}$ data plotted against B/Ca, Mg/Ca, Sr/Ca and U/Ca trace
721 element composition. Symbols represent fibre sampling technique as in Figure 3. Error bars
722 show the 2σ external reproducibility. *D* values (*e.g.* Gaetani and Cohen, 2006) refer to the
723 approximate partition coefficient of each trace element into aragonite (D_X =
724 $(X/Ca)_{Aragonite}/(X/Ca)_{Seawater}$). R^2 values are representative of the linear regression of just the
725 milled/drilled samples (*i.e.* excluding laser cut samples with anomalously high B/Ca).

726

727 Figure 6: Rayleigh fractionation models for Mg, Sr, and B incorporation into *D. dianthus*
728 (*e.g.* Gagnon et al., 2007). Panels A and B show theoretical coral Rayleigh fractionation
729 curves for respectively, Mg/Ca *vs* Sr/Ca and B/Ca *vs* $\delta^{11}B$ as [Ca] in the ECF reduces. We
730 show the impact of changing initial elemental concentration of ECF (e.g. $[Sr]_{Initial\ ECF}$ +5%,
731 −5% and −15%) and partition coefficients (*D*). The calcifying fluid assumptions are: $[Ca]_{sw}$
732 = 10.3 mM; $[Sr]_{sw}$ = 91 µM; $[Mg]_{sw}$ = 52.8 mM; $[B]_{sw}$ = 432.6 µM; $\delta^{11}B_{sw}$ = 39.61

μmol/kg; α_B = 1.0272; pK_B^* = 8.79; internal pH = 8.62. Data for *D. dianthus* specimens in this study with many replicates (19168, 45669, and 47413) are plotted to show their fit to the Rayleigh fractionation models. Squares represent fibre replicates taken sequentially from the same fibre band (19168 this study; Figure 4; and 47407; Gagnon et al., 2007). Fibre replicates taken from different septa within the samples are shown as circles. The shaded region of panel B represents the impact of active Ca^{2+} pumping into the ECF replacing up to 10% of the Ca^{2+} lost to $CaCO_3$ precipitation.

Table 1: *D. dianthus* specimens used in this study and previously measured boron isotope data for bulk *D. dianthus* (Anagnostou et al., 2012). Proximal hydrographic bottle data are from the CDIAC ocean carbon system database. Additional carbonate system parameters based on specimen location are calculated using SeaCarb R package.

Table 2: Fibrous aragonite *D. dianthus* $\delta^{11}B$ and trace element data. Measured $\delta^{11}B$ data are corrected for the effect of the measured total procedural blank (TPB). Sampling method symbols correspond to those in Figure 3.

Table 3: Trace element results of cleaned/uncleaned bulk sample 19168 crushed by pestle and mortal and JCp-1 powdered coral standard. Results of uncleaned JCp-1 are compared to the interlaboratory comparison study by Hathorne et al., (2013). All uncleaned JCp-1 results are within the robust standard deviation of Hathorne et al., (2013) with the exception of Sr/Ca for which a correction factor of 1.047 must be applied to Sr/Ca results in this study.

Table 4: Regression summary of *D. dianthus* fibrous aragonite (this study) and bulk septa (Anagnostou et al., 2012) calibrations. Regression in the form $\delta^{11}B_{coral} = m \times \delta^{11}B_{borate} + c$ presented with one standard error uncertainties.

7 References

Adkins, J.F., Henderson, G.M., Wang, S.L., O'Shea, S., Mokadem, F., 2004. Growth rates of the deep-sea scleractinia *Desmophyllum cristagalli* and *Enallopsammia rostrata*. Earth and Planetary Science Letters, 227(3–4): 481-490.

Al-Horani, F.A., Al-Moghrabi, S.M., de Beer, D., 2003a. The mechanism of calcification and its relation to photosynthesis and respiration in the scleractinian coral Galaxea fascicularis. Marine Biology, 142(3): 419-426.

Al-Horani, F.A., Al-Moghrabi, S.M., de Beer, D., 2003b. Microsensor study of photosynthesis and calcification in the scleractinian coral, Galaxea fascicularis: active internal carbon cycle. Journal of Experimental Marine Biology and Ecology, 288(1): 1-15.

Allemand, D. et al., 2004. Biomineralisation in reef-building corals: from molecular mechanisms to environmental control. Comptes Rendus Palevol, 3(6–7): 453-467.

Allison, N., Finch, A.A., EIMF, 2010. δ^{11}B, Sr, Mg and B in a modern Porites coral: the relationship between calcification site pH and skeletal chemistry. Geochimica et Cosmochimica Acta, 74(6): 1790-1800.

Anagnostou, E., Huang, K.F., You, C.F., Sikes, E.L., Sherrell, R.M., 2012. Evaluation of boron isotope ratio as a pH proxy in the deep sea coral *Desmophyllum dianthus*: Evidence of physiological pH adjustment. Earth and Planetary Science Letters, 349–350(0): 251-260.

Anagnostou, E. et al., 2011. Seawater nutrient and carbonate ion concentrations recorded as P/Ca, Ba/Ca, and U/Ca in the deep-sea coral Desmophyllum dianthus. Geochimica et Cosmochimica Acta, 75(9): 2529-2543.

Barker, S., Greaves, M., Elderfield, H., 2003. A study of cleaning procedures used for foraminiferal Mg/Ca paleothermometry. Geochemistry Geophysics Geosystems, 4(9): 8407.

Barker, S., Knorr, G., Vautravers, M.J., Diz, P., Skinner, L.C., 2010. Extreme deepening of the Atlantic overturning circulation during deglaciation. Nature Geosci, 3(8): 567-571.

Blamart, D. et al., 2007. Correlation of boron isotopic composition with ultrastructure in the deep-sea coral Lophelia pertusa: Implications for biomineralization and paleo-pH. Geochemistry, Geophysics, Geosystems, 8(12): Q12001.

Burke, A., Robinson, L.F., 2012. The Southern Ocean's Role in Carbon Exchange During the Last Deglaciation. Science, 335(6068): 557-561.

Cairns, S.D., 1994. Scleractinia of the temperate North Pacific. Smithsonian Institution Press.

Cheng, H., Adkins, J., Edwards, R.L., Boyle, E.A., 2000. U-Th dating of deep-sea corals. Geochimica et Cosmochimica Acta, 64(14): 2401-2416.

Cohen, A.L., McConnaughey, T.A., 2003. Geochemical Perspectives on Coral Mineralization. Reviews in Mineralogy and Geochemistry, 54(1): 151-187.

Comeau, S., Carpenter, R.C., Edmunds, P.J., 2013. Coral reef calcifiers buffer their response to ocean acidification using both bicarbonate and carbonate. Proceedings of the Royal Society B: Biological Sciences, 280(1753).

D'Olivo, J.P., McCulloch, M.T., Eggins, S.M., Trotter, J., 2015. Coral records of reef-water pH across the central Great Barrier Reef, Australia: assessing the influence of river runoff on inshore reefs. Biogeosciences, 12(4): 1223-1236.

Dickson, A.G., 1990. Thermodynamics of the dissociation of boric acid in synthetic seawater from 273.15 to 318.15 K. Deep Sea Research Part A. Oceanographic Research Papers, 37(5): 755-766.

Dodds, L.A., Roberts, J.M., Taylor, A.C., Marubini, F., 2007. Metabolic tolerance of the cold-water coral Lophelia pertusa (Scleractinia) to temperature and dissolved oxygen change. Journal of Experimental Marine Biology and Ecology, 349(2): 205-214.

Doney, S.C., Fabry, V.J., Feely, R.A., Kleypas, J.A., 2009. Ocean Acidification: The Other CO2 Problem. Annual Review of Marine Science, 1(1): 169-192.

Douville, E. et al., 2010. Rapid and accurate U–Th dating of ancient carbonates using inductively coupled plasma-quadrupole mass spectrometry. Chemical Geology, 272(1–4): 1-11.

Farmer, J.R., Hönisch, B., Robinson, L.F., Hill, T.M., 2015. Effects of seawater-pH and biomineralization on the boron isotopic composition of deep-sea bamboo corals. Geochimica et Cosmochimica Acta, 155(0): 86-106.

Försterra, G., Beuck, L., Häussermann, V., Freiwald, A., 2005. Shallow-water Desmophyllum dianthus (Scleractinia) from Chile: characteristics of the biocoenoses, the bioeroding community, heterotrophic interactions and (paleo)-bathymetric implications. In: Freiwald, A., Roberts, J.M. (Eds.), Cold-Water Corals and Ecosystems. Erlangen Earth Conference Series. Springer Berlin Heidelberg, pp. 937-977.

Foster, G.L., 2008. Seawater pH, pCO_2 and [CO_3^{2-}] variations in the Caribbean Sea over the last 130 kyr: A boron isotope and B/Ca study of planktic foraminifera. Earth and Planetary Science Letters, 271(1-4): 254-266.

Foster, G.L., Pogge von Strandmann, P.A.E., Rae, J.W.B., 2010. Boron and magnesium isotopic composition of seawater. Geochemistry, Geophysics, Geosystems, 11(8): Q08015.

Gabitov, R.I., Gaetani, G.A., Watson, E.B., Cohen, A.L., Ehrlich, H.L., 2008. Experimental determination of growth rate effect on U6+ and Mg2+ partitioning between aragonite and fluid at elevated U6+ concentration. Geochimica et Cosmochimica Acta, 72(16): 4058-4068.

Gaetani, G.A., Cohen, A.L., 2006. Element partitioning during precipitation of aragonite from seawater: A framework for understanding paleoproxies. Geochimica et Cosmochimica Acta, 70(18): 4617-4634.

Gagnon, A.C., Adkins, J.F., Erez, J., 2012. Seawater transport during coral biomineralization. Earth and Planetary Science Letters, 329–330(0): 150-161.

Gagnon, A.C., Adkins, J.F., Fernandez, D.P., Robinson, L.F., 2007. Sr/Ca and Mg/Ca vital effects correlated with skeletal architecture in a scleractinian deep-sea coral and the role of Rayleigh fractionation. Earth and Planetary Science Letters, 261(1–2): 280-295.

Gattuso, J.-P., Epitalon, J.-M., Lavigne, H., 2015. Seacarb: Seawater Carbonate Chemistry. R package version 3.0.6 .http://CRAN.R-project.org/package=seacarb.

Guinotte, J.M. et al., 2006. Will human-induced changes in seawater chemistry alter the distribution of deep-sea scleractinian corals? Frontiers in Ecology and the Environment, 4(3): 141-146.

Gutjahr, M. et al., 2014. Boron Isotope Intercomparison Project (BIIP): Development of a new carbonate standard for stable isotopic analyses. Geophysical Research Abstracts, EGU General Assembly 2014, 16(EGU2014-5028-1).

Hathorne, E.C. et al., 2013. Interlaboratory study for coral Sr/Ca and other element/Ca ratio measurements. Geochemistry, Geophysics, Geosystems, 14(9): 3730-3750.

Hemming, N.G., Hanson, G.N., 1992. Boron Isotopic Composition and Concentration in Modern Marine Carbonates. Geochimica et Cosmochimica Acta, 56(1): 537-543.

Hemming, N.G., Hönisch, B., 2007. Boron Isotopes in Marine Carbonate Sediments and the pH of the Ocean. In: Hillaire–Marcel, C., de Vernal, A. (Eds.), Developments in Marine Geology. Elsevier, pp. 717-734.

Henehan, M.J. et al., 2013. Calibration of the boron isotope proxy in the planktonic foraminifera Globigerinoides ruber for use in palaeo-CO2 reconstruction. Earth and Planetary Science Letters, 364(0): 111-122.

Hoegh-Guldberg, O. et al., 2007. Coral Reefs Under Rapid Climate Change and Ocean Acidification. Science, 318(5857): 1737-1742.

Holcomb, M., Cohen, A.L., Gabitov, R.I., Hutter, J.L., 2009. Compositional and morphological features of aragonite precipitated experimentally from seawater and biogenically by corals. Geochimica et Cosmochimica Acta, 73(14): 4166-4179.

Holcomb, M., DeCarlo, T.M., Gaetani, G.A., McCulloch, M., 2016. Factors affecting B/Ca ratios in synthetic aragonite. Chemical Geology, 437: 67-76.

Holcomb, M. et al., 2015. Cleaning and pre-treatment procedures for biogenic and synthetic calcium carbonate powders for determination of elemental and boron isotopic compositions. Chemical Geology, 398: 11-21.

Hönisch, B., Bickert, T., Hemming, N.G., 2008. Modern and Pleistocene boron isotope composition of the benthic foraminifer Cibicidoides wuellerstorfi. Earth and Planetary Science Letters, 272(1–2): 309-318.

Hönisch, B. et al., 2004. Assessing scleractinian corals as recorders for paleo-pH: Empirical calibration and vital effects. Geochimica et Cosmochimica Acta, 68(18): 3675-3685.

Hönisch, B. et al., 2012. The Geological Record of Ocean Acidification. Science, 335(6072): 1058-1063.

Kiss, E., 1988. Ion-exchange separation and spectrophotometric determination of boron in geological materials. Analytica Chimica Acta, 211: 243-256.

Klochko, K., Kaufman, A.J., Yao, W., Byrne, R.H., Tossell, J.A., 2006. Experimental measurement of boron isotope fractionation in seawater. Earth and Planetary Science Letters, 248(1–2): 276-285.

Krief, S. et al., 2010. Physiological and isotopic responses of scleractinian corals to ocean acidification. Geochimica et Cosmochimica Acta, 74(17): 4988-5001.

873 Lee, K. et al., 2010. The universal ratio of boron to chlorinity for the North Pacific and North Atlantic
874 oceans. Geochimica et Cosmochimica Acta, 74(6): 1801-1811.

875 Lemarchand, E., Schott, J., Gaillardet, J., 2005. Boron isotopic fractionation related to boron sorption
876 on humic acid and the structure of surface complexes formed. Geochimica et Cosmochimica Acta,
877 69(14): 3519-3533.

878 Lomitschka, M., Mangini, A., 1999. Precise Th/U-dating of small and heavily coated samples of deep
879 sea corals. Earth and Planetary Science Letters, 170(4): 391-401.

880 Lueker, T.J., Dickson, A.G., Keeling, C.D., 2000. Ocean pCO_2 calculated from dissolved inorganic
881 carbon, alkalinity, and equations for K_1 and K_2: validation based on laboratory measurements of CO_2
882 in gas and seawater at equilibrium. Marine Chemistry, 70: 105-119.

883 Martínez-Botí, M.A. et al., 2015. Boron isotope evidence for oceanic carbon dioxide leakage during
884 the last deglaciation. Nature, 518(7538): 219-222.

885 Mavromatis, V., Montouillout, V., Noireaux, J., Gaillardet, J., Schott, J., 2015. Characterization of
886 boron incorporation and speciation in calcite and aragonite from co-precipitation experiments under
887 controlled pH, temperature and precipitation rate. Geochimica et Cosmochimica Acta, 150(0): 299-
888 313.

889 McConnaughey, T., 1989. ^{13}C and ^{18}O isotopic disequilibrium in biological carbonates: I. Patterns.
890 Geochimica et Cosmochimica Acta, 53(1): 151-162.

891 McCulloch, M., Falter, J., Trotter, J., Montagna, P., 2012a. Coral resilience to ocean acidification and
892 global warming through pH up-regulation. Nature Clim. Change, 2(8): 623-627.

893 McCulloch, M. et al., 2012b. Resilience of cold-water scleractinian corals to ocean acidification:
894 Boron isotopic systematics of pH and saturation state up-regulation. Geochimica et Cosmochimica
895 Acta, 87(0): 21-34.

896 Mienis, F. et al., 2014. Cold-water coral growth under extreme environmental conditions, the Cape
897 Lookout area, NW Atlantic. Biogeosciences, 11(9): 2543-2560.

898 Montagna, P. et al., 2014. Li/Mg systematics in scleractinian corals: Calibration of the thermometer.
899 Geochimica et Cosmochimica Acta, 132(0): 288-310.

900 Montagna, P., McCulloch, M., Taviani, M., Remia, A., Rouse, G., 2005. High-resolution trace and
901 minor element compositions in deep-water scleractinian corals (Desmophyllum dianthus) from the
902 Mediterranean Sea and the Great Australian Bight. In: Freiwald, A., Roberts, J.M. (Eds.), Cold-Water
903 Corals and Ecosystems. Erlangen Earth Conference Series. Springer Berlin Heidelberg, pp. 1109-1126.

904 Mortensen, P.B., Hovland, T., Fosså, J.H., Furevik, D.M., 2001. Distribution, abundance and size of
905 Lophelia pertusa coral reefs in mid-Norway in relation to seabed characteristics. Journal of the Marine
906 Biological Association of the United Kingdom, 81(04): 581-597.

907 Noireaux, J. et al., 2015. Crystallographic control on the boron isotope paleo-pH proxy. Earth and
908 Planetary Science Letters, 430: 398-407.

909 Okai, T., Suzuki, A., Kawahata, H., Terashima, S., Imai, N., 2002. Preparation of a New Geological
910 Survey of Japan Geochemical Reference Material: Coral JCp-1. Geostandards Newsletter, 26(1): 95-
911 99.

912 Orr, J.C. et al., 2005. Anthropogenic ocean acidification over the twenty-first century and its impact on
913 calcifying organisms. Nature, 437(7059): 681-686.

914 Rae, J.W.B., Foster, G.L., Schmidt, D.N., Elliott, T., 2011. Boron isotopes and B/Ca in benthic
915 foraminifera: Proxies for the deep ocean carbonate system. Earth and Planetary Science Letters, 302(3-
916 4): 403-413.

917 Reynaud, S., Hemming, N.G., Juillet-Leclerc, A., Gattuso, J.-P., 2004. Effect of pCO_2 and temperature
918 on the boron isotopic composition of the zooxanthellate coral Acropora sp. Coral Reefs, 23(4): 539-
919 546.

920 Roberts, J.M., Wheeler, A.J., Freiwald, A., 2006. Reefs of the Deep: The Biology and Geology of
921 Cold-Water Coral Ecosystems. Science, 312(5773): 543-547.

922 Rollion-Bard, C., Blamart, D., 2014. SIMS method and examples of applications in coral
923 biomineralization. In: DiMasi, E., Gower, L.B. (Eds.), Biomineralization Sourcebook: Characterization
924 of Biominerals and Biomimetic Materials. CRC Press, pp. 249.

925 Sabine, C.L. et al., 2004. The Oceanic Sink for Anthropogenic CO_2. Science, 305(5682): 367-371.

926 Sanyal, A. et al., 1996. Oceanic pH Control on the Boron Isotopic Composition of Foraminifera:
927 Evidence from Culture Experiments. Paleoceanography, 11(5): 513-517.

928 Sanyal, A., Nugent, M., Reeder, R.J., Bijma, J., 2000. Seawater pH control on the boron isotopic
929 composition of calcite: evidence from inorganic calcite precipitation experiments. Geochimica et
930 Cosmochimica Acta, 64(9): 1551-1555.

931 Schlitzer, R., 2015. Ocean Data View, http://odv.awi.de.

932 Skinner, L.C., Fallon, S., Waelbroeck, C., Michel, E., Barker, S., 2010. Ventilation of the Deep
933 Southern Ocean and Deglacial CO_2 Rise. Science, 328(5982): 1147-1151.

934 Stanley, G.D., Cairns, S.D., 1988. Constructional azooxanthellate coral communities; an overview
935 with implications for the fossil records. Palaios, 3(2): 233-242.

936 Stoll, H., Langer, G., Shimizu, N., Kanamaru, K., 2012. B/Ca in coccoliths and relationship to
937 calcification vesicle pH and dissolved inorganic carbon concentrations. Geochimica et Cosmochimica
938 Acta, 80: 143-157.

939 Tambutté, S. et al., 2011. Coral biomineralization: From the gene to the environment. J Exp Mar Biol
940 Ecol, 408: 58-78.

941 Thiagarajan, N., Subhas, A.V., Southon, J.R., Eiler, J.M., Adkins, J.F., 2014. Abrupt pre-Bolling-
942 Allerod warming and circulation changes in the deep ocean. Nature, 511(7507): 75-78.

943 Thresher, R.E., Adkins, J., Thiagarajan, N., 2011. Modal analysis of the deep-water solitary
944 scleractinian, *Desmophyllum dianthus*, on SW Pacific seamounts: inferred recruitment periodicity,
945 growth, and mortality rates. Coral Reefs, 30(4): 1063-1070.

946 Trotter, J. et al., 2011. Quantifying the pH 'vital effect' in the temperate zooxanthellate coral
947 *Cladocora caespitosa*: Validation of the boron seawater pH proxy. Earth and Planetary Science
948 Letters, 303(3–4): 163-173.

Venn, A.A. et al., 2013. Impact of seawater acidification on pH at the tissue–skeleton interface and calcification in reef corals. Proceedings of the National Academy of Sciences, 110(5): 1634-1639.

Watson, E.B., 2004. A conceptual model for near-surface kinetic controls on the trace-element and stable isotope composition of abiogenic calcite crystals1. Geochimica et Cosmochimica Acta, 68(7): 1473-1488.

Yu, J. et al., 2010. Loss of Carbon from the Deep Sea Since the Last Glacial Maximum. Science, 330(6007): 1084-1087.

Zeebe, R.E., Wolf-Gladrow, D.A., 2001. CO_2 in seawater: equilibrium, kinetics, isotopes, 65. Elsevier, Elsevier Oceanography Series, Amsterdam, The Netherlands, 360 pp.

Figure1

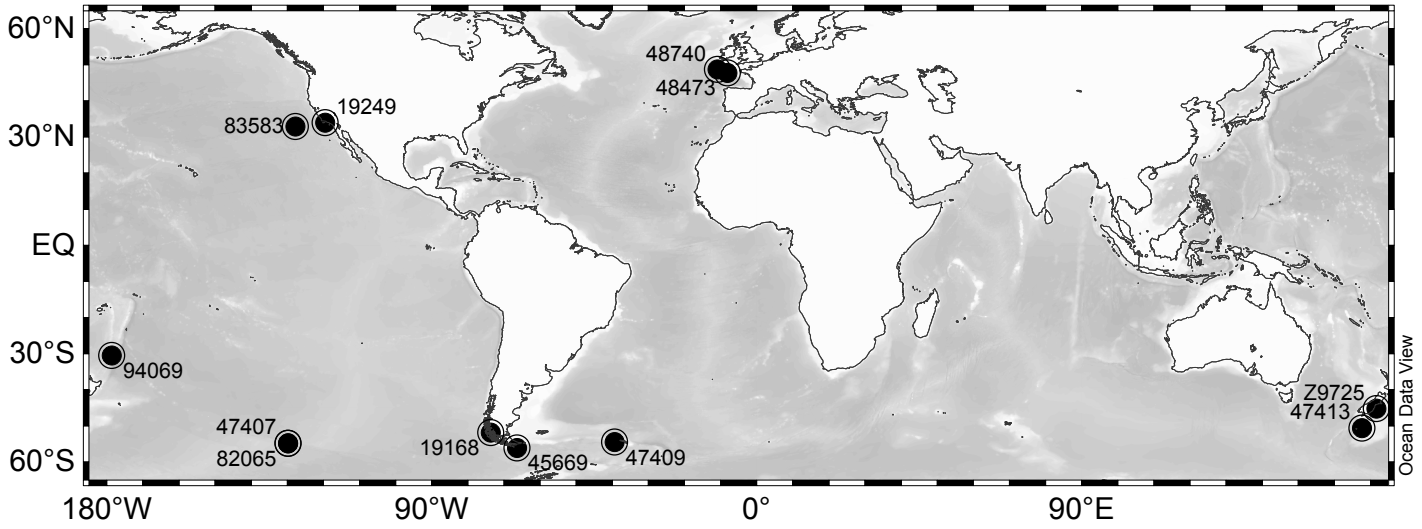

Figure 1: Locations of the D. dianthus specimens used in this study. Map created using Ocean Data View software (R. Schlitzer, 2015, http://odv.awi.de)

Figure2

Figure 2: Sampling of DSC fibrous aragonite. Panel A: Sectioning of DSC septa to expose target fibrous aragonite along with centres of calcification (COC) and edge coatings. Light microscope image of coral sample 19186 used in this study. Panels B, C and D show different sampling techniques of polished sections described in the text. Microdrilling (B): direct drilling of fibres using fine drill bit to collect powdered sample. Micromilling (C): drilling and initial sampling trench (green) before milling towards fibre samples (yellow) using broad drill bit. Laser cutting (D): repeated laser shots are used to cut whole fibre section from a thin section of 200µm thickness.

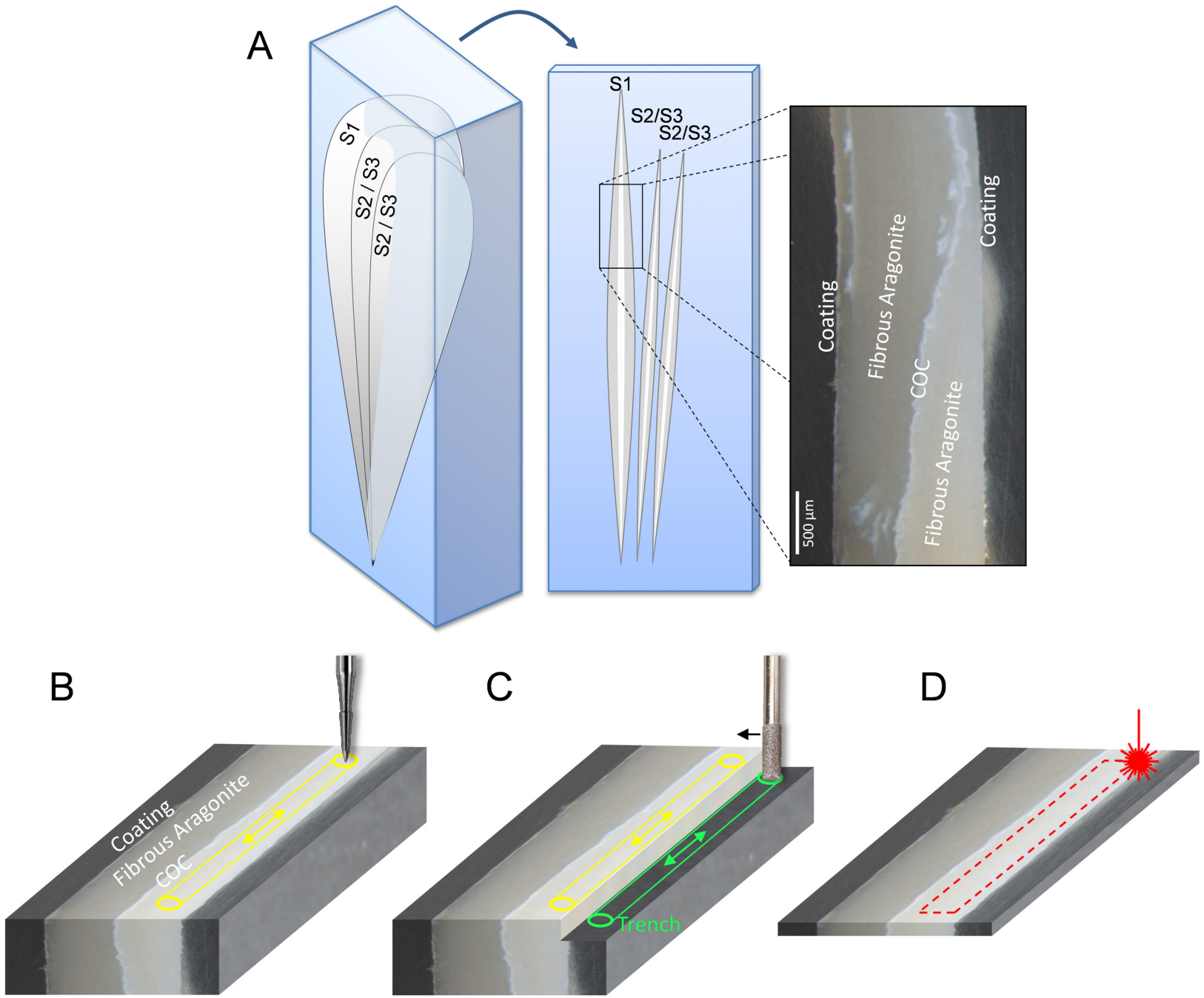

Figure3

Figure 3: Measured $\delta^{11}B$ of coral regressed against the $\delta^{11}B_{borate}$ of ambient seawater. Panel A. $\delta^{11}B$ of bulk *D. dianthus* (Anagnostou et al., 2012), tropical corals (Hönisch et al., 2004; Krief et al., 2010; Reynaud et al., 2004; Trotter et al., 2011), and bamboo coral (Farmer et al., 2015). Grey dashed parallel lines in show 1:1 $\delta^{11}B$ relationship and the same relationship offset by +11‰. Panel B. (inset of A) shows new fibrous aragonite *D. dianthus* data in comparison to bulk *D. dianthus* (Anagnostou et al., 2012). Open blue symbols represent drilled (triangles), milled (circles) and laser cut fibres (crosses) sampling techniques (error bars show 2σ of each replicate). Filled blue symbols highlight the *D. dianthus* fibre replicate with the lowest Mg/Ca. Regression lines are least squares regression models and their 95% confidence intervals (shaded envelopes) for bulk and low Mg/Ca fibre data.

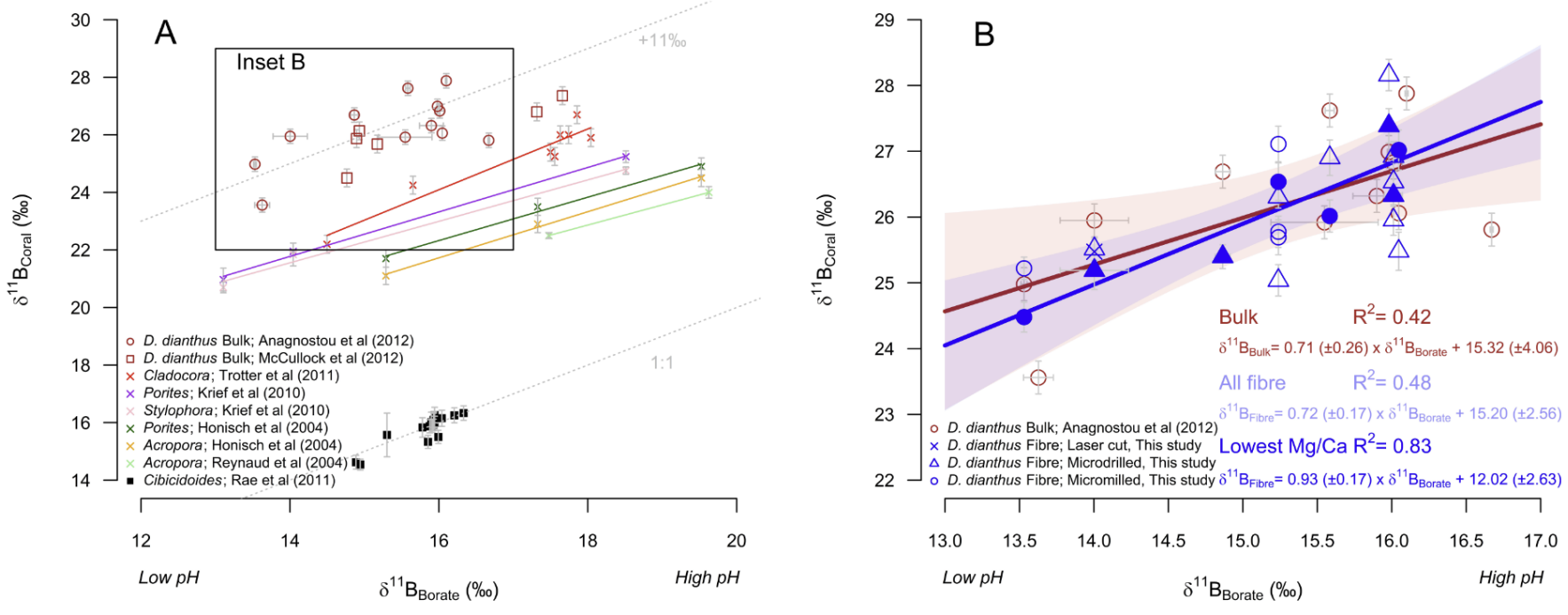

Figure4

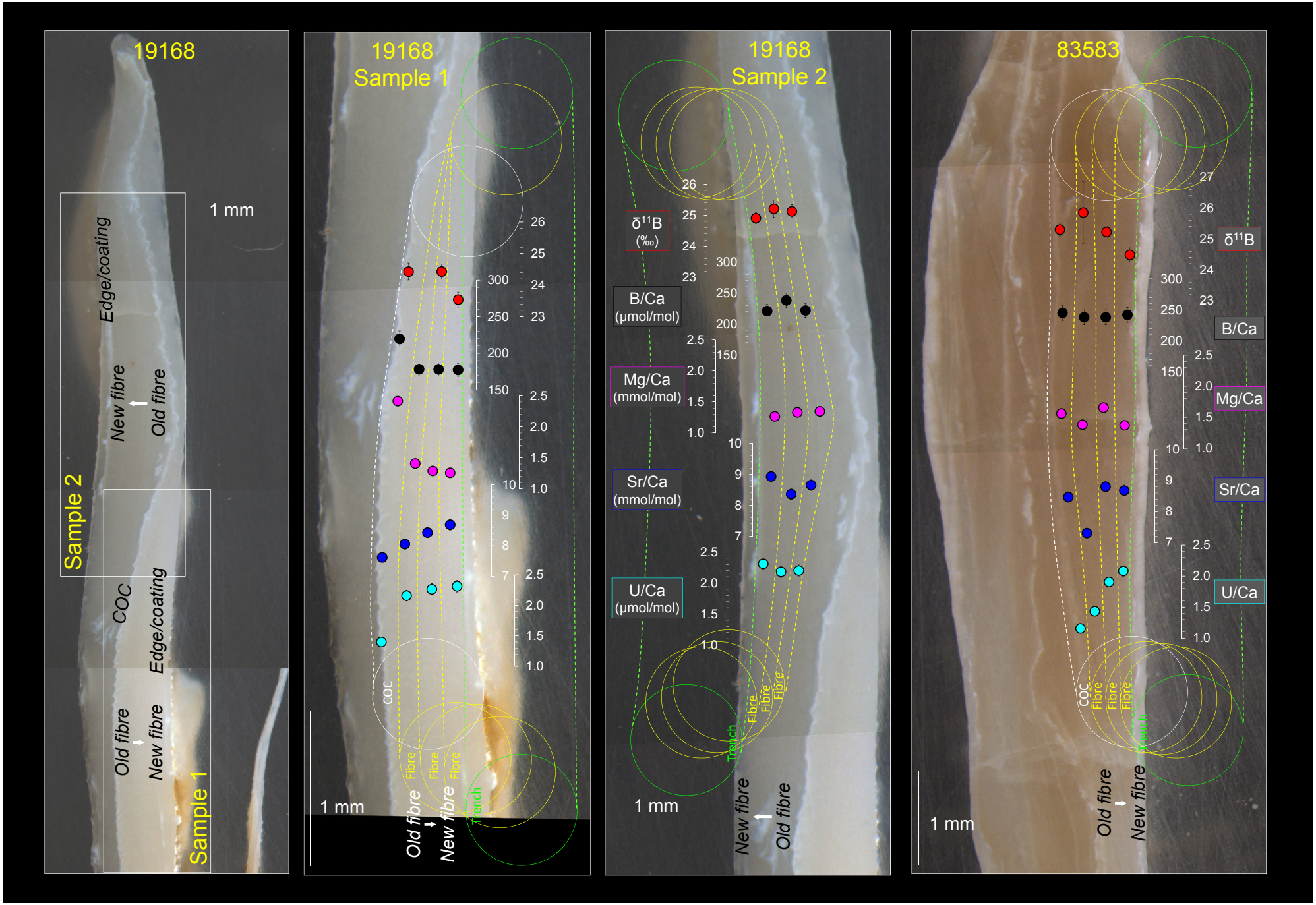

Figure 4: $\delta^{11}B$ and trace metal composition across bands of fibrous aragonite in *D. dianthus* corals 19168 and 83583 (low pH site) sampled by micromilling from presumed newest to oldest fibre growth. The positions of sample trenches are highlighted in green; subsequent samples are then shown in yellow. The positions where COC samples were also taken are delineated by the connected white circles.

Figure5

Figure 5: *D. dianthus* $\delta^{11}B_{fibre}$ data plotted against B/Ca, Mg/Ca, Sr/Ca and U/Ca trace element composition. Symbols represent fibre sampling technique as in Figure 3. Error bars show the 2σ external reproducibility. *D* values (e.g. Gaetani and Cohen, 2006) refer to the approximate partition coefficient of each trace element into aragonite ($D_X = (X/Ca)_{Aragonite}/(X/Ca)_{Seawater}$). R^2 values are representative of the linear regression of just the milled/drilled samples (i.e. excluding laser cut samples with anomalously high B/Ca).

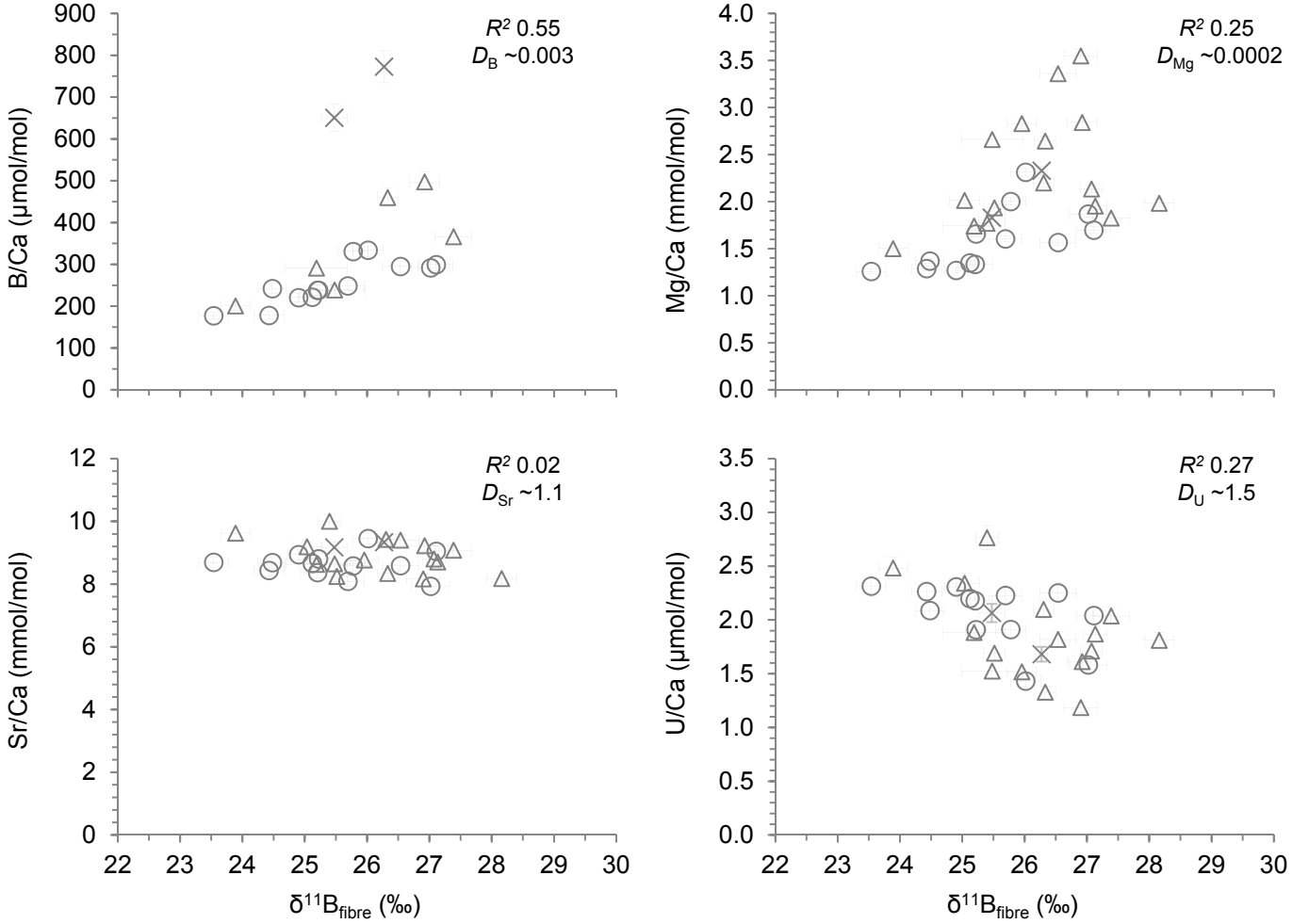

Figure6

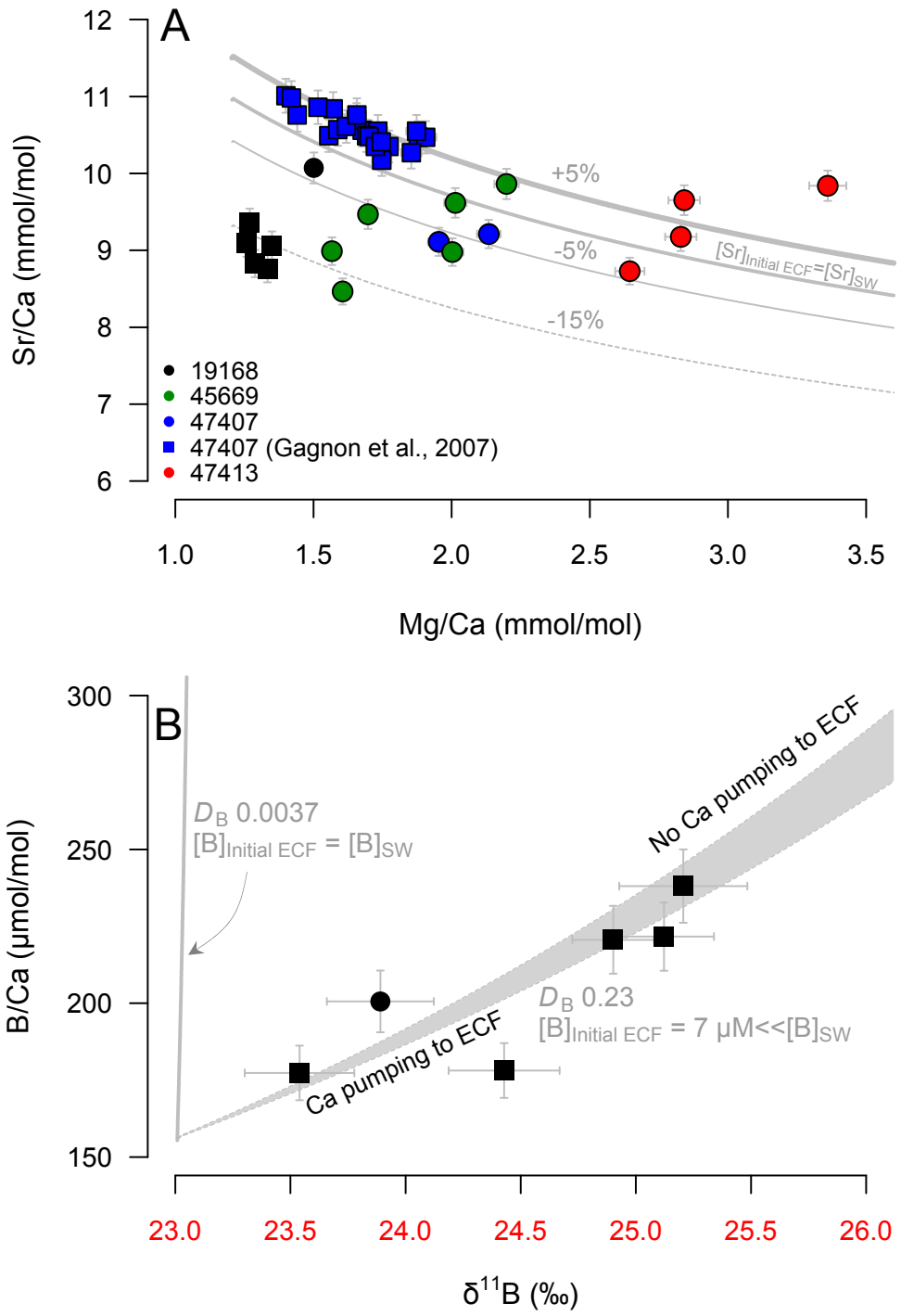

Figure 6: Rayleigh fractionation models for Mg, Sr, and B incorporation into *D. dianthus* (e.g. Gagnon et al., 2007). Panels A and B show theoretical coral Rayleigh fractionation curves for respectively, Mg/Ca vs Sr/Ca and B/Ca vs $\delta^{11}B$ as [Ca] in the ECF reduces. We show the impact of changing initial elemental concentration of ECF (e.g. [Sr]Initial ECF +5%, −5% and −15%) and partition coefficients (*D*). The calcifying fluid assumptions are: $[Ca]_{sw}$ = 10.3 mM; $[Sr]_{sw}$ = 91 µM; $[Mg]_{sw}$ = 52.8 mM; $[B]_{sw}$ = 432.6 µM; $\delta^{11}B_{sw}$ = 39.61 µmol/kg; α_B = 1.0272; pK_B^* = 8.79; internal pH = 8.62. Data for *D. dianthus* specimens in this study with many replicates (19168, 45669, and 47413) are plotted to show their fit to the Rayleigh fractionation models. Squares represent fibre replicates taken sequentially from the same fibre band (19168 this study; Figure 4; and 47407; Gagnon et al., 2007). Fibre replicates taken from different septa within the samples are shown as circles. The shaded region of panel B represents the impact of active Ca^{2+} pumping into the ECF replacing up to 10% of the Ca^{2+} lost to CaCO3 precipitation.

Table1

Click here to download Table: Table 1 Hydro..pdf

Table 1: *D. dianthus* specimens used in this study and previously measured boron isotope data for bulk *D. dianthus* (Anagnostou et al., 2012). Proximal hydrographic bottle data are from the CDIAC ocean carbon system database. Additional carbonate system parameters based on specimen location are calculated using SeaCarb R package.

					Hydrographic bottle data										Calculated: SeaCarb R package						
Coral ID	Lat (°N)	Long (°E)	Coral Depth (m)	Coral Year	Data Repository	Cruise	Station	Hydro-graphic Year	Bottle Depth (m)	Temp (°C)	Salinity (PSU)	$[PO_4^{3-}]$ (µM)	$[SiO_4^{2-}]$ (µM)	Total Alkalinity (µmol/kg)	DIC (µmol/kg)	Seawater pH (Total)	$[CO_3^{2-}]$ (µmol/kg)	Ω_{Arag}	pK_B^*	Seawater $\delta^{11}B_{borate}$ (‰)	Uncert. $\delta^{11}B_{borate}$ (‰)	Anagnostou et al., (2012) $\delta^{11}B_{Bulk}$ (‰)
19168	-51.9	-73.7	636	1888	Unavailable																	25.91
19249	34.0	-119.5	274	1889	WOCE	P02T	85	1994	297.4	7.8	34.11	2.35	43.70	2271	2226	7.69	57	0.83	8.80	14.00	0.23	25.95
45669	-56.1	-66.4	439	1963	GEOSECS	NA	76	1972	384.0	1.3	34.19	2.18	38.90	2313	2195	8.00	92	1.28	8.87	15.24	0.02	-
47407	-54.8	-129.8	549	1964	Unavailable																	24.96
47409	-54.5	-39.4	672.5	1966	WOCE	A16S	277	1989	789.0	1.8	34.69	2.23	92.81	2336	2238	7.91	82	1.08	8.85	14.86	0.02	26.69
47413	-50.6	167.6	421	1964	WOCE	P15S	66	1996	369.7	5.9	34.26	1.52	8.81	2284	2124	8.05	116	1.63	8.81	16.01	0.06	26.83
48473	47.7	-8.1	1107	1973	WOCE	A24	32	1997	1096.5	8.5	35.55	1.11	10.66	2348	2182	7.97	121	1.50	8.74	16.05	0.00	26.06
48739	47.6	-7.3	825	1973	WOCE	A24	32	1997	799.3	9.6	35.53	1.05	8.90	2344	2172	7.98	126	1.64	8.74	16.10	0.01	27.88
48740	48.7	-10.9	1470	1973	WOCE	A24	32	1997	1490.3	5.1	35.12	1.18	14.03	2324	2169	7.99	112	1.28	8.76	15.98	0.01	26.99
62309	40.4	-67.7	522	1979	WOCE	A22	73	1997	495.7	6.1	35.05	1.38	21.10	2317	2179	7.97	105	1.43	8.80	15.55	0.36	25.92
78630	46.8	-130.8	312	1982	WOCE	P01	105	2007	327.4	5.8	33.96	2.63	61.71	2280	2265	7.61	45	0.65	8.82	13.63	0.10	23.56
80358	48.0	-7.8	358	1967	WOCE	A24	33	1997	350.3	11.0	35.54	0.62	3.95	2336	2129	8.06	148	2.11	8.74	16.67	0.01	25.81
82065	-54.8	-129.8	585.5	1964	Unavailable																	25.49
83583	32.9	-127.8	464	1986	WOCE	P02T	83	1994	498.7	5.8	34.10	2.88	68.70	2290	2284	7.57	42	0.59	8.81	13.53	0.02	24.98
94069	-30.5	-178.7	710	1993	WOCE	P06W	191	2003	694.0	7.4	34.49	1.61	12.10	2284	2146	7.95	104	1.38	8.78	15.58	0.03	27.62
Z9725	-45.2	171.6	276	1999	WOCE	P15S	77	1996	326.9	8.1	34.51	1.35	7.17	2288	2130	8.01	117	1.68	8.79	15.90	0.16	26.32

Table2

Click here to download Table: Table 2 Chem data..pdf

Table 2: Fibrous aragonite *D. dianthus* $\delta^{11}B$ and trace element data. Measured $\delta^{11}B$ data are corrected for the effect of the measured total procedural blank (TPB). Sampling method symbols correspond to those in Figure 3.

Coral ID	Sample mass (mg)	Total mass of fibre samples (mg)	Measured $\delta^{11}B_{fibre}$ Replicates (‰)	**$\delta^{11}B_{fibre}$ (‰) (TPB corr.)**		±2σ	**$\delta^{11}B_{fibre}$ Average (‰)**	2SD of average	$\delta^{11}B_{COC\ or\ Coat}$ (‰) (TPB corr.)	±2σ	B/Ca (µmol/mol)	Mg/Ca (mmol/mol)	Al/Ca (µmol/mol)	Fe/Ca (µmol/mol)	Mn/Ca (µmol/mol)	Sr/Ca ‡ (mmol/mol)	U/Ca (µmol/mol)	Sampling method
19168	0.66	2.53	23.82	**23.89**		0.23	**24.51**	1.37			201	1.50	13	0	1	10.07	2.48	○ MicroDrilled
	0.56		24.84	**24.90**		0.18					221	1.27	16	5	3	9.36	2.31	△ MicroMilled
	0.12		24.98	**25.21**		0.28					238	1.33	22	2	5	8.76	2.18	△ MicroMilled
	0.43		25.02	**25.12**		0.22					222	1.35	10	1	2	9.06	2.20	△ MicroMilled
	0.43		23.43	**23.54**	†	0.24					177	1.26	3	1	4	9.10	2.31	△ MicroMilled
	0.34		24.30	**24.43**		0.24					178	1.29	8	0	2	8.83	2.26	△ MicroMilled
19168 COC	0.20	Not included in $\delta^{11}B$-pH calibration							24.43	0.27	220	2.42	16	3	3	7.98	1.40	△ MicroMilled
19249	0.13	0.77	24.95	**25.19**	†	0.50	**25.39**	0.36			291	1.74	65	0	12	9.03	1.88	○ MicroDrilled
	0.42		25.47	**25.52**		0.17					-	1.94	14	4	1	8.63	1.69	○ MicroDrilled
	0.22		25.40	**25.47**		0.21					650	1.83	40	5	1	9.60	2.06	× Laser cut
45669	0.39	1.44	26.26	**26.31**		0.17	**26.08**	0.08			-	2.20	30	16	1	9.86	2.10	○ MicroDrilled
	0.23		24.95	**25.04**		0.24					-	2.01	71	60	3	9.62	2.34	○ MicroDrilled
	0.27		25.54	**25.69**		0.26					249	1.61	192	28	2	8.47	2.23	△ MicroMilled
	0.30		25.67	**25.78**		0.24					331	2.00	65	65	2	8.98	1.91	△ MicroMilled
	0.07		26.31	**26.54**	†	0.29					295	1.57	38	17	2	8.99	2.25	△ MicroMilled
	0.18		26.93	**27.11**		0.27					300	1.70	17	10	2	9.47	2.04	△ MicroMilled
47407	0.45	0.83	27.08	**27.13**	†	0.18	**27.10**	0.01			-	1.95	18	9	2	9.11	1.87	○ MicroDrilled
	0.38		27.02	**27.07**		0.18					-	2.13	21	9	2	9.21	1.71	○ MicroDrilled
47409	0.36	0.36	25.35	**25.40**	†	0.18	**25.40**				-	1.77	26	22	5	10.47	2.76	○ MicroDrilled
47413	0.27	0.92	26.82	**26.92**		0.24	**26.44**	0.10			497	2.84	113	0	3	9.65	1.61	○ MicroDrilled
	0.31		26.29	**26.33**	†	0.17					460	2.64	5	3	1	8.73	1.33	○ MicroDrilled
	0.28		25.87	**25.96**		0.23					-	2.83	27	7	1	9.18	1.52	○ MicroDrilled
	0.06		26.32	**26.54**		0.29					-	3.36	100	5	3	9.84	1.82	○ MicroDrilled
47413Coating	0.17	Not included in $\delta^{11}B$-pH calibration							23.95	0.24	-	2.81	105	8	2	9.86	1.60	○ MicroDrilled
48473	0.14	0.25	25.24	**25.48**		0.49	**26.25**	0.27			239	2.66	62	0	2	9.05	1.52	○ MicroDrilled
	0.11		26.70	**27.02**	†	0.30					292	1.87	37	7	2	8.30	1.58	△ MicroMilled
48740	0.26	0.48	27.23	**27.39**	†	0.30	**27.77**	0.08			366	1.83	22	0	1	9.50	2.04	○ MicroDrilled
	0.23		28.06	**28.16**		0.24					-	1.98	66	40	6	8.56	1.81	○ MicroDrilled
82065	0.45	0.45	26.24	**26.27**	†	0.10	**26.27**				773	2.33	6	42	1	9.77	1.68	× Laser cut
83583	0.35	0.90	24.37	**24.48**	†	0.23	**24.85**	0.08			242	1.37	9	4	0	9.09	2.09	△ MicroMilled
	0.55		25.16	**25.22**		0.17					238	1.66	8	4	0	9.22	1.91	△ MicroMilled
	0.05		25.24	**25.85***		1.00					238	1.38	83	9	2	7.65	1.43	△ MicroMilled
83583 COC	0.38	Not included in $\delta^{11}B$-pH calibration							25.30	0.20	245	1.56	7	3	0	8.87	1.16	△ MicroMilled
94069	0.14	0.41	26.76	**26.90**		0.27	**26.46**	0.04			-	3.55	80	49	34	8.55	1.18	○ MicroDrilled
	0.26		25.90	**26.02**	†	0.24					334	2.31	11	30	16	9.90	1.43	△ MicroMilled
94069Coating	0.29	Not included in $\delta^{11}B$-pH calibration							25.78	0.22	-	3.39	168	218	79	8.57	1.41	○ MicroDrilled

* Sample mass too small for inclusion in $\delta^{11}B$-pH calibration

† Replicate with lowest Mg/Ca

‡ Correction factor applied (× 1.047) based on results of JCp-1 standard

Table3

Click here to download Table: Table 3 Cleaning..pdf

Table 3: Trace element results of cleaned/uncleaned bulk sample 19168 crushed by pestle and mortal and JCp-1 powdered coral standard. Results of uncleaned JCp-1 are compared to the interlaboratory comparison study by Hathorne et al., (2013). All uncleaned JCp-1 results are within the robust standard deviation of Hathorne et al., (2013) with the exception of Sr/Ca for which a correction factor of 1.047 must be applied to Sr/Ca results in this study.

	Sample	**Oxidative cleaned**		**B/Ca (µmol/mol)**	Impact of oxidative cleaning	**Mg/Ca (mmol/mol)**	Impact of oxidative cleaning	**U/Ca (µmol/mol)**	Impact of oxidative cleaning	**Sr/Ca (mmol/mol)**	Impact of oxidative cleaning
This study (n = 3)	Bulk 19168 (Pestle and mortar)	Yes	Average	**510**	0%	**1.90**	0%	**2411**	-2%	**10.04**	0%
			%RSD	2		2		3		0	
This study (n = 6)	Bulk 19168 (Pestle and mortar)	No	Average	**509**		**1.91**		**2461**		**10.07**	
			%RSD	1		4		3		1	
This study (n = 4)	JCp-1 (Fine powder)	Yes	Average	**325**	-26%	**3.15**	-24%	**1245**	4%	**8.47**	0%
			%RSD	2		1		2		0.7	
This study (n = 4)	JCp-1 (Fine powder)	No	Average	**438**	✓ within robust SD	**4.14**	✓	**1196**	✓	**8.44**	✗ corr. factor 1.047
			%RSD	2		2		3		0.2	
Hathorne et al., (2013)	JCp-1 (Fine powder)	No	Robust average	**460**		**4.20**		**1192**		**8.84**	
			Robust SD	23		0.07		45.00		0.04	

Table4

Click here to download Table: Table 4 regression..pdf

Table 4: Regression summary of *D. dianthus* fibrous aragonite (this study) and bulk septa (Anagnostou et al., 2012) calibrations. Regression in the form $\delta^{11}B_{coral} = m \times \delta^{11}B_{borate} + c$ presented with one standard error uncertainties.

		Slope		Intercept		
D. dianthus data set		*m*	1SE	*c*	1SE	R^2
Bulk	(Anagnostou et al., 2012)	0.71	(±0.26)	15.32	(±4.06)	**0.42**
All Fibre	(This study)	0.72	(±0.17)	15.20	(±2.56)	**0.48**
Average Fibre	(This study)	0.78	(±0.21)	14.32	(±3.22)	**0.69**
Average Fibre weighted by sample mass	(This study)	0.75	(±0.17)	14.69	(±2.57)	**0.76**
Low Mg/Ca Fibre	(This study)	0.93	(±0.17)	12.02	(±2.63)	**0.83**